Technische Universiteit
Eindhoven
University of Technology

Department of Mechanical Engineering
Sustainable Energy Technology Master Program
Energy Technology Group

The potential of electricity storage by high temperature heat storage within the Ecovat context

Master Thesis

Chris Kwikkers

Supervisor:
Dr. Ir. Camilo Rindt

Examination committee members:
Dr. Ir. Michel Speetjens
Dr. Madeleine Gibescu

Eindhoven, June 2018

Contents

List of variables

Symbol	Unit	Variable
Ap	$[m]$	Pipe circumference
AU	$[W/(m^2/K)]$	Overall heat transfer coefficient
C	$[kJ/K]$	Heat capacity
c	$[kJ/(kg \cdot K)]$	Specific heat capacity
d	$[m]$	Diameter
E	$[J]$	Energy
f	$[-]$	Friction factor
H	$[J]$	Enthalpy
$h_{\#}$	$[J/kg]$	Specific enthalpy
h	$[W/(m^2 \cdot K)]$	Heat transfer coefficient
L	$[m]$	Length
k	$[W/(m \cdot K)]$	Thermal conductivity
m	$[kg]$	Mass
$\dot{m}$	$[kg/s]$	Mass flow
n	$[-]$	Number of pipes
P	$[W]$	Power
Q	$[J]$	Thermal energy
R	$[m]$	Outer radius
r	$[m]$	Radius
S	$[J/K]$	Entropy
s	$[J/(K \cdot kg)]$	Specific entropy
SP	$[-]$	Size parameter
T	$[K]$	Temperature
t	$[s]$	Time
u	$[m/s]$	Bulk flow velocity
V	$[m^3]$	Volume
W	$[J]$	Useful work
x	$[m]$	Distance from inner diameter
z	$[m]$	Distance from entrance pipe
α	$[m^2/s]$	Thermal diffusion coefficient
ϵ	$[\%]$	Effectiveness
η	$[\%]$	Efficiency
ρ	$[kg/m^3]$	Density

List of Figures

Chapter 1

Introduction

1.1 The need for electricity storage

The European Commission has introduced an energy roadmap to 2050 to combat climate change. This roadmap states that by 2050 the CO2 emissions of the European Union should be at 5% of the emissions of the year 1990 [6]. To achieve this it is necessary to shift from fossil fuel energy sources to more renewable ones such as wind and solar. This shift to renewables has a profound effect on the European energy system. Due to the intermittent and unpredictable behavior of renewable energy sources, the stability of the electrical grid and reliability of energy supply are at risk. To combat these problems energy buffers can be implemented, absorbing excess energy and supplying energy when production is not sufficient. For this purpose, Ecovat has developed a sensible heat storage system. Ecovat designs and manufactures underground seasonal heat storage tanks, using a passive, stratified water tank principle. The system is charged using heat pumps and electric heaters during the spring and summer. Charging is done at times when electricity supplied by the grid is abundant and cheap. By absorbing the excess electricity the Ecovat system can be used to balance the electricity grid and lower the curtailment of renewables. Due to its large size and good insulation, the heat can be stored for long periods of time with minimal losses. During the colder months the system is discharged to supply its customers with heat for central heating and direct hot water purposes. Currently Ecovat is conducting validation experiments on their 70 MWh test location and developing their first full scale commercial project.

In the current configuration an Ecovat system is only able to store energy asymmetrically, absorbing electricity and supplying heat. However, in light of the changing energy system Ecovat is interested in the possibilities to incorporate symmetrical storage into their system. The ability to store electricity symmetrically opens up a number of additional applications such as electric load shifting and improving power quality and reliability.

Several techniques for stationary electrical energy storage are currently implemented in a variety of applications. Most of these applications are used for emergency power or are used in combination with some sort of (renewable) energy generation. In these combinations the purpose of the electricity storage is to complement the power generation in the form of curve smoothing or expanding the time of operation. The performance of the different techniques varies greatly on aspects such as response time, power, storage capacity, operating temperature etc. Therefore, the technique which is used is strongly dependent on the desired application. In addition, boundary conditions influence the efficiency or applicability of any given technique. An example of such a boundary condition is the availability of, or demand for, waste energy streams like saturated steam or low temperature heat. Other boundary conditions might limit certain techniques to locations with very specific geographical attributes such as mountains or underground aquifers.

The initial focus of Ecovat was on short term storage of electricity, and utilize the short term fluctuations in electricity price and balance prices to achieve a feasible business case. After a preliminary analysis of the short term fluctuations in electricity prices it was concluded that, with current prices and technology it was not economically feasible to implement electricity storage for short term storage. Therefore it was decided to focus more on bulk energy storage for providing reliability of supply in an energy system with diminishing reliability.

Long term bulk electrical energy storage can be achieved using several approaches. Currently the most widely implemented form of electricity storage are: pumped hydro storage and electrochemical storage in the form of Lithium-ion batteries. In this report the focus will be on storing electricity using high temperature heat storage (HTS). This focus was chosen because of the possible synergy HTS has with the existing Ecovat system.

1.2 Problem definition and research question

Due to the energy transition towards renewables the energy system is expected to change and with it the need for new services is expected to develop. Due to the intermittent and unpredictable behavior of renewable energy sources electricity storage is needed to maintain the current reliability of supply. Furthermore, electricity storage can be used for services such as preventing curtailment, power quality control and preventing congestion issues. The goal of this master thesis is to determine the possibilities for symmetrical electricity storage within the existing Ecovat by implementing high temperature storage. This goal has led to the following research question:

How can symmetrical electricity storage in the form of high temperature storage be integrated within the Ecovat system to meet future energy system needs?

1.3 Approach

The research question focuses on the needs of the developing energy system therefore the first step is to determine these needs. It is not an aim of this thesis to reach an economically competitive solution, but the demands of a future energy system will be used to determine performance indicators for the system. To make this assessment future scenarios of the energy market will be analyzed and possible applications for storage within these scenarios are determined.

To correctly identify the solution which has the highest potential in combination with the Ecovat system a comparative study will be conducted. The different energy conversion and storage options are compared on several technical and economic aspects, with as key indicators thermal efficiency, profitability and practicality. To correctly asses the performance on these key indicators firstly more fundamental aspects of the technology need to be determined. These include but are not limited to:

- Storage capacity
- Storage density
- Discharging power
- Discharging efficiency
- Cost

After the configuration has been determined. a numerical model is constructed to model the discharging behavior. A parameter study is conducted to assess the impact of parameter deviations on the performance of the system. Lastly the profitability of the system is assessed when compared to alternatives and no electricity storage unit.

Chapter 2

Energy storage background and techniques

In this chapter the developing need for large scale electricity storage is elaborated upon. Firstly, the current demand for services which can be performed by electricity storage are discussed, as well as the way in which these are met now. Secondly, the effects of the changing energy system on the need for electricity storage are discussed in further detail. Lastly, it is discussed how these factors impact the design of the system.

2.1 Electricity storage

Network scale Electricity storage has been used for decades to perform, amongst others, peak shaving and flexibility services. However, due to the rise of renewable energy sources interest has grown over the last number of years. This has led to many new projects being developed, and new technologies are now being considered for these applications.

2.2 Current demand for flexibility

As mentioned in the introduction, the changing European energy system calls for novel techniques to alleviate the problems caused by unpredictable and intermittent electricity sources. Even though the scale on which these problems will occur is new, in essence the problems of imbalanced energy systems and a mismatch between supply and demand are not. Currently the flexibility services to deal with these problems are mainly performed by supply side management, fluctuating the output of power plants. However, fluctuating the output power does diminish the efficiency of electricity generation. Therefore demand side management is also implemented in the form of grid scale electricity storage.

The techniques used for grid scale electricity storage can be split into two categories: power to power (P2P) and power to heat (P2H). P2P storage refers to systems which charge using electricity and also supply electricity while discharging. P2H systems are also charged using electricity but supply heat while discharging. The energy storage system proposed in this report is a P2P system, as the distinction between the categories is made in terms of system output not storage principle.

Currently P2P systems are used for flexibility operations such as power balancing and peak shaving for conventional power plants, frequency control and emergency power. Numerous different techniques exist to preform these operations, an overview of these is given in figure 2.1. The extent to which the most prevalent of these technologies are implemented is shown in figure 2.2.

Different technologies are more suited for different applications depending on their performance characteristics. Among these characteristics power rating and rated discharge time are some of the most significant. These dictate what powers can be delivered and for how long, which is an indication of the total storage capacity. A summary of these parameters is given in figure 2.3. The techniques which are used most in current applications are discussed in the next paragraph.

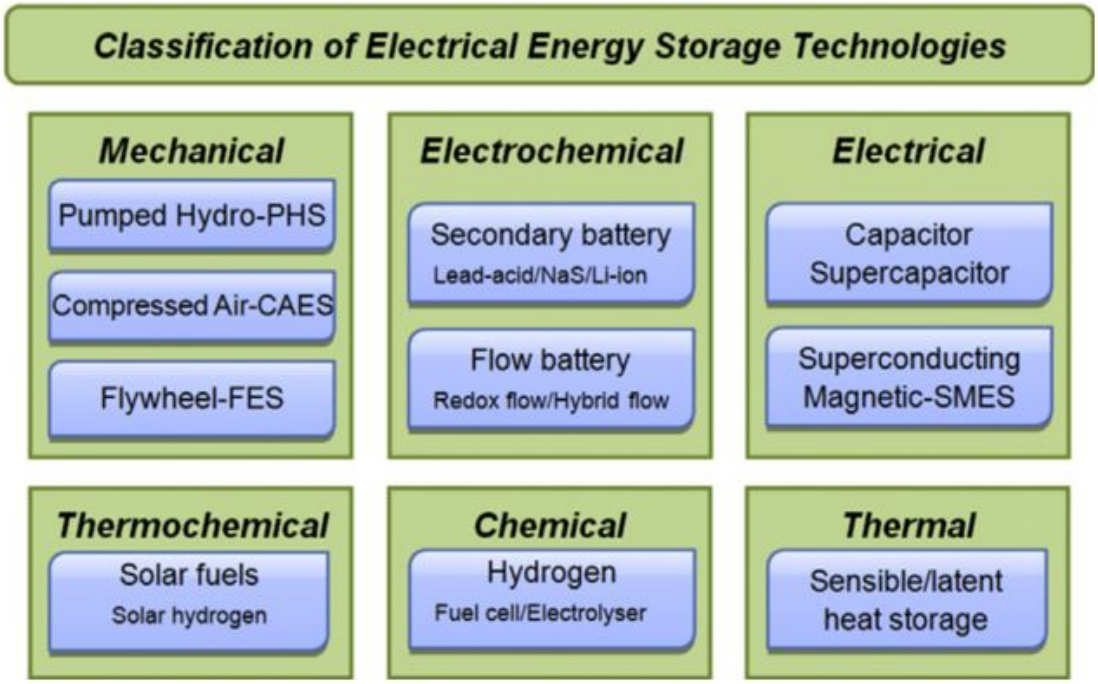

Figure 2.1: Electrical energy storage technologies [11]

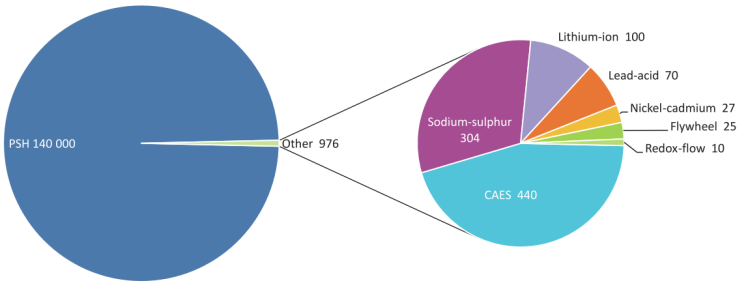

Figure 2.2: Installed capacity energy storage technologies,[5]

	Power rating (MW)	Discharge time	Cycles, or lifetime	Self-discharge	Energy density (Wh/l)	Power density (W/l)	Efficiency	Response time
Pumped Hydro	100 – 2500	4 – 16h	30 – 60 years	~ 0	0.2 – 2	0.1 – 0.2	70 – 85%	10 s – min
Compressed Air	10 – 1000	2 – 30h	20 – 40 years	~ 0	2 – 6	0.2 – 0.6	40 – 70%	min
Flywheels	0.001 – 20	sec – min	20000 – 100000	1.3 – 100%	20 – 80	5000	70 – 95%	< sec
Li-ion battery	0.05 – 100	1 min – 8h	1000 – 10000	0.1 – 0.3%	200 – 400	1300 – 10000	85 – 95%	< sec
Lead-acid battery	0.001-100	1 min – 8h	6 – 40 years	0.1 – 0.3%	50 – 80	90 - 700	80 – 90%	< sec
Sodium-sulphur battery	10 – 100	1 min – 8h	2500 – 4500	0.05 – 20%	150 – 300	120 – 160	70 – 90%	< sec
Flow battery	0.1 – 100	hours	12000 – 14000	0.2%	20 – 70	0.5 – 2	60 – 85%	< sec
Superconducting Magnetic	0.1 – 1	ms – sec	100000	10 – 15%	~ 6	~ 2600	80 – 95%	< sec
Supercapacitor	0.01 – 1	ms – min	10000 – 100000	20 – 40%	10 – 20	40000 - 120000	80 – 95%	< sec
Hydrogen	0.01 – 100	min – week	5 – 30 years	0 – 4%	600 (200bar)	0.2 – 20	25 – 45%	sec - min
Synthetic Natural Gas	1 – 100	hour – week	30 years	Negligible	1800 (200bar)	0.2 – 2	25 – 50%	sec - min
Molten Salt (latent thermal)	1 – 150	hours	30 years	n/a	70 – 210	n/a	80 – 90%	min

Figure 2.3: Technological parameters of electricity storage technologies [21]

2.3 Current applications electricity storage

By far the most implemented form of P2P energy storage is pumped hydro storage (PHS). PHS systems consist of two water reservoirs located at different heights, connected by a system of pipes. During charging water is pumped from the lower reservoir to the higher reservoir, storing the energy in the form of gravitational potential energy. During the discharging phase the water in the higher reservoir is dropped to the lower reservoir. The high velocity falling water is fed through a turbine connected to a generator which generates electricity. A schematic representation of such an installation is shown in figure 2.4. The efficiency which can be achieved using PHS varies between 70-80%. The total globally installed power of PHS exceeds 140 GW, accounting for more than 98% of P2P storage installed power. Roughly half of this installed power is installed in Japan, China and the US [22]. Because the amount of energy which can be stored in the system scales with the height difference between the low and the high basin, a large height differential is desired between the two, typically 200-300 meters. Furthermore, due to the low energy density of PHS a large body of water is needed to store a functional amount of energy, typically 10^7 cubic meters. PHS systems are therefore built in hilly or mountainous regions with (artificial) lakes, making the viability of such systems geographically limited. These constraints cause PHS systems to have large investment costs and have long construction times. The investment costs are offset by low operational costs, given that the plant is able to operate over a sufficiently long time span. PHS systems are primarily used to balance fossil fuel power plants and to provide peak power, they are therefore designed at large power levels, up to 3000 MW. Because the energy is stored in the form of gravitational energy self discharge is low making PHS suited for storage on longer time scales.

Even though most PHS projects were realized many years ago, the push for a less carbon intensive energy system has revamped industry interest. This has led to the development of new methods such as salt water PHS. However, due to the impact that PHS has on the environment in which it is implemented the suitability of PHS needs to be judged on a case to case bases. Therefore, the role that PHS will play in the future energy infrastructure will differ greatly per country.[22].

2.3.1 Compressed air energy storage

The second largest P2P storage technique is compressed air energy storage (CAES). When using this technique air is compressed and stored at hight pressure. During discharge the compressed air is expanded over a turbine to generate electricity. Due to the low losses during storage this technique is especially suited for long term storage. The efficiency of the system can be improved by storing the heat created during compression, and use this heat to improve the efficiency of the expansion process. The air can be stored in either: purpose built pressure vessels or existing geological structures. However due to the high cost of the pressure vessels storage in existing geological structures is preferred from an economic standpoint. This limits the number of possible applications of the technique. A variation on CAES is Liquefied Air Energy Storage (LAES), where the air is stored in its liquid form at atmospheric pressure. To achieve this the air needs to be cooled to -196 degrees centigrade and stored in an insulated tank. This allows for a very compact storage tank, but to cool the air large additional equipment needs to be installed. This makes this option less suited for small scale applications.

2.3.2 Flywheel energy storage

At the other end of the spectrum lie technologies which are less suited for long term storage but have very short response times. An example of such a technology is a flywheel which stores the energy as rotational kinetic energy of a wheel spinning inside a vacuum chamber. Flywheels have a very short reaction time, meaning that they can start discharging quickly after the demand arises. This fast reaction time makes them especially suited for voltage/frequency regulation and ramping

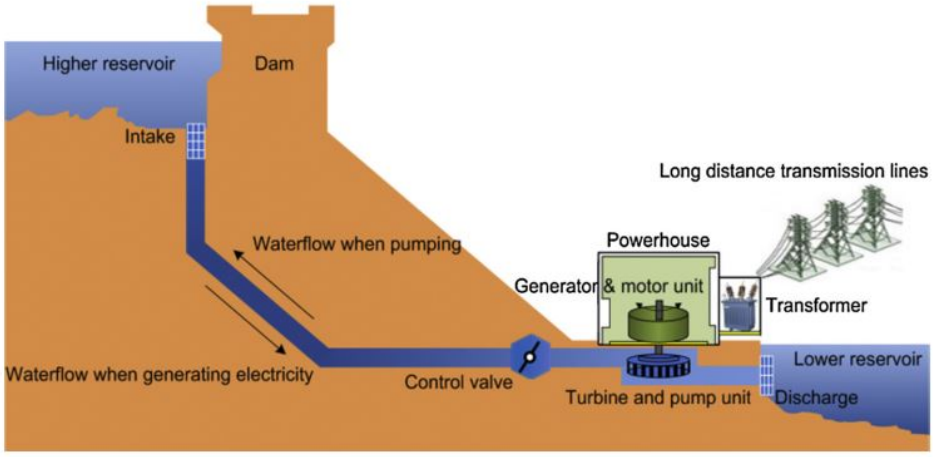

Figure 2.4: Representation of PHS plant [11]

services. The energy storage density of flywheels is low. As a consequence of this, and their main application as voltage regulation, the total amount of installed storage capacity is low. This in combination with their large self-discharge over time makes them unsuited for energy storage over longer periods of time.

2.3.3 Batery energy storage

Electrochemical energy storage, or battery energy storage (BES), is currently the third largest technique for P2P storage. It is however the fastest growing storage technique, in particular lithium ion (Li-Ion) batteries show a large increase in projects and fast diminishing production costs. Batteries consist of several electrochemical cells which are connected in series/parallel to achieve the desired voltage and power characteristics. The voltage in each cell is produced by an electrochemical reaction between an anode, a cathode and an electrolyte which serves as the transport medium for the charge carriers. Depending on the combination of these three components, batteries have different characteristics suited for different applications. Functions performed by BES range from power quality, to energy management, to transportation. Batteries have short response times in the range of milliseconds making them suited for power quality control. BES have relatively high cycle efficiencies in comparison with other storage techniques. The main barriers for large scale BES systems are the low cycling times, the number of times the system can be charged and discharged, and their high maintenance costs. The combination of cathode, anode and electrolyte material greatly influences the performance characteristics of batteries. The combinations which have the greatest potential for bulk electricity storage are discussed below. The information in the next section has been gathered from an overview paper on electrical energy storage technologies [11].

Lithium ion (Li-Ion)
These batteries have good power density in comparison with other batteries. This makes lithium ion batteries suited for applications where small dimensions and low weight of equipment are important. This has led to their adoption in mobile applications such as electric vehicles and small electronics batteries. However, Li-Ion batteries have also been implemented in several utility scale projects. Current research focusses on further increasing battery power and storage capacity.

Sodium Sulphur (NaS)
The main advantages of NaS batteries are their low self-discharge, cheap materials and high capacity. However due to the use of molten sodium as its electrolyte, NaS batteries have a

high internal temperature of 574-624 K. This leads to high operating costs and the need for a temperature control system. Despite these difficulties NaS batteries are considered as one of the most promising candidates for bulk electrical energy storage. Currently there is one company which manufactures large scale NaS batteries for electrical energy storage which is situated in Japan. Production was halted briefly in 2012 after one of their battery systems had caught fire during operation, production has resumed since then. Research is currently focused on increasing cell performance and lowering operating temperature.

Sodium Nickel Chloride (NaNiCl)
The NaNiCl is similar to the NaS battery as they both use molten sodium as their electrolyte and both operate at high temperatures. NaNiCl batteries have moderate performance with respect to power and storage density but require no maintenance, have very little self-discharge and good pulsed power capabilities. Despite these advantages few companies have adopted and developed the NaNiCl principle.

Flow battery energy storage (FBES)
With conventional batteries the capacity and power of a cell are correlated. Therefore combinations such as a large capacity with low power are not practical which leads to expensive system and unused power capabilities. Flow batteries do not have this problem due to the use of liquid cathodic and anodic materials. This allows flow batteries to be adapted too specific applications and avoid unneeded costs. Furthermore, due to the fact that the materials are liquid they can be stored separately leading to very low self-discharge during storage.

2.4 Future markets electricity storage

How the demand for electricity storage will develop in the future is dependent on the development of the energy supply. To investigate this DNV-GL, an energy consulting company, in cooperation with the TU Delft and Berenschot has used energy system scenarios made by the European network of transmission system operators of electricity (ENTSOE) to predict future price fluctuations and demand for flexibility. The results of this study have been outlined in the report Roadmap Energystorage 2030 published in 2013 and the information in the following section is taken from that report [4]. The report outlines four possible scenarios for how the Dutch electricity system might adapt. Furthermore, the report analyses the expected demand for flexibility caused by these four scenarios and its impact on electricity prices. The four scenarios which are used in the report are outlined below.

High sustainability CHP with 20 GW solar and wind
This scenario is characterized by moderate implementation of solar and wind with flexible CHP plants to balance the system. This system requires low amounts of must run gas turbine balancing plants.

ENTSO-E vision 3 with 20 GW solar and wind
This scenario contains the same amount implemented solar and wind but with fewer flexible CHPs to balance the system. This calls for a larger amount of must run gas turbine plants to balance the system. This leads to a large surplus of energy at times when solar and wind energy is abundant.

ENTSO-E vision 4+ with 30 GW solar and wind
Similar to the previous scenario but with even more installed solar and wind. The increased share of renewables aggravates the problems encountered in the previous scenario, large amount of must run gas turbines and large surpluses.

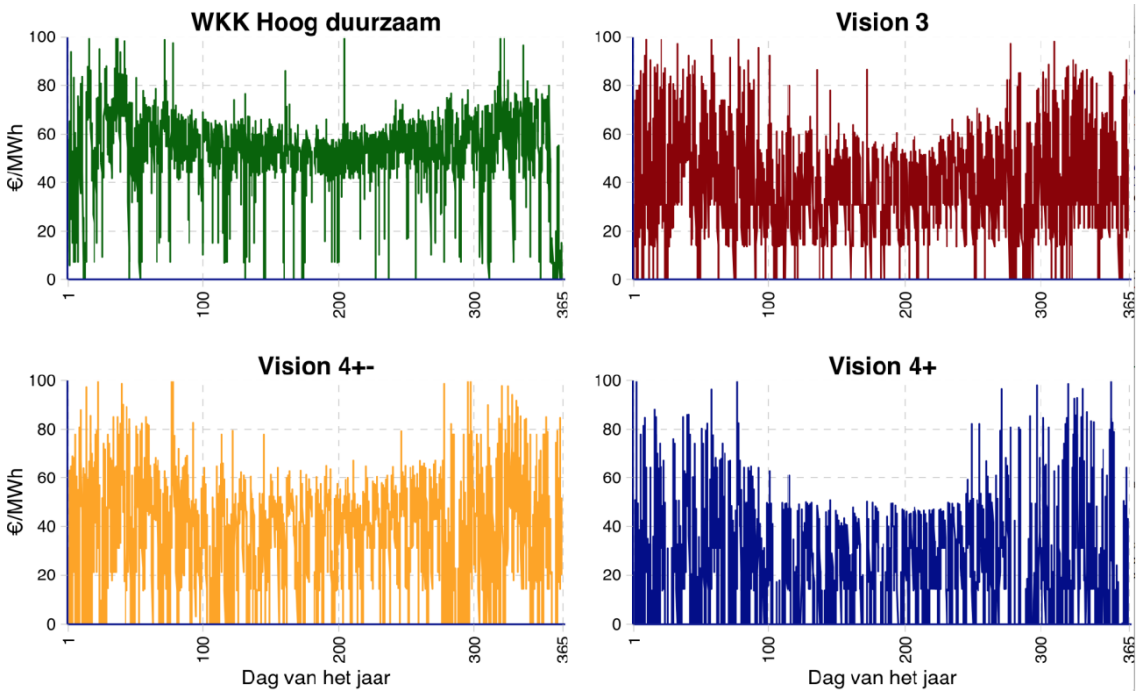

Figure 2.5: Expected electricity price fluctuations for different ENTSOE scenarios [4]

ENTSO-E vision 4+- with 30 GW solar and wind
A variation on the Vision 4+ scenario with the addendum that fewer must run gas turbines are included. This leads to lower must run gas turbine power but a larger share of CHP plants.

The expected price fluctuations which arise from these scenarios are shown in figure 2.5. From the figure it can be concluded that as the share of renewables increases the overall price decrease as the price volatility increases. Note that the number of instances where the electricity price approaches zero increases as well along with the share of renewables.

Aside from the price fluctuations it was also studied at what intervals large fluctuations in power were expected to arise. As well as the amount of storage capacity needed to meet the storage demand at each of these time intervals. This data is shown in figures 2.6 and 2.7. In these graphs the ENTSO-E vision 4 scenario (the green line) is compared to the base load, as well as to scenarios in which with other renewables are implemented. From the first graph it can be concluded that all scenarios lead to larger fluctuations in power in comparison with the base load. A notable exception to this is the daily interval where the scenarios which employ a mix of renewables have smaller fluctuations in comparison with the base case. The larger power fluctuations are in accordance with the reasoning that larger shares of renewables will lead to larger power fluctuations on time scales not related to either human activity (daily) or meteorologically (annual cycles). This point is also reflected in the second chart where the demand for storage capacity deviates from the base load especially on time scales between one day and one year.

2.4.1 Arbitrage

Due to the fluctuations in electricity price over time, storage can be used to store cheaply bought electricity until it can be sold for a higher price. This process of buying low and selling high is similar to trading on the stock market and is referred to by a term borrowed from the stock market: arbitrage. Electricity can be bought or sold by pledging to consume or produce a certain amount

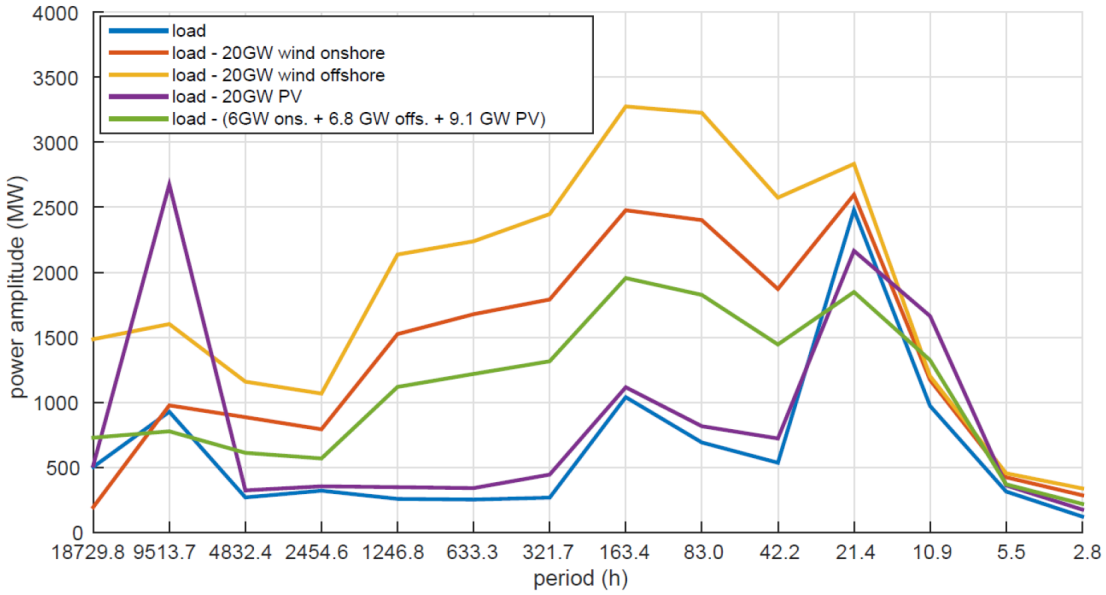

Figure 2.6: Spectral representation of expected power fluctuations in several scenarios [4]

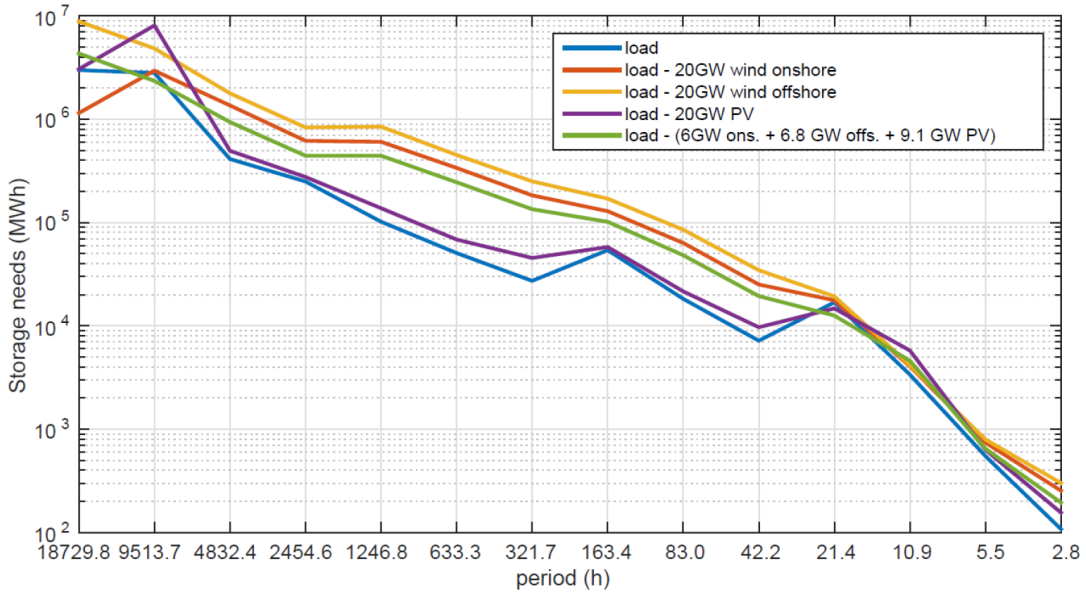

Figure 2.7: Needed storage capacity per timescale to meet supply/demand mismatch [4]

of power for a number of Program Time Units (PTUs). Every hour is divided up into four PTUs of fifteen minutes each. Electricity units can be traded on the long term, day ahead, intraday and balancing markets. DNV-GL used the scenarios and current pricing data to determine the impact of the different scenarios on the future electricity prices of the different markets.

Long term and day ahead markets
These two markets refer to the buying and selling of PTU obligations before the producing and consumption for that day has been locked in. The long term market refers to trading occurring more than one day before the execution date, this time period can be as long as months or years. The day ahead market refers to the trade of energy to be delivered the next day, markets close the day before. For the day ahead market the report concludes that the volatility increases for all scenarios, the most for scenarios with large shares of renewables. This increase in volatility manifests itself in an increase in the number of price fluctuations, not the magnitude of the price differences. The most frequent price differential between hours was up to 20 EUR/MWh, these typically occurred on a time scale of six to twelve hours. This suggests a possibly profitable option for shorter charge/discharge cycles. One problem of trading on the day ahead market is that because all bids must be done in advance, traders have little certainty when trading on longer time scales.

Intraday market
The intraday market refers to the trading of energy within 36 hours before the energy is supplied or demanded, the intraday is typically more volatile than the day ahead market. On the intraday market the volatility increases further in the scenario's evaluated by DNV-GL, with both more and greater price fluctuations. This makes it a more viable option for storage arbitrage. Furthermore, because traders can alter their bids up to five minutes before the dispatch time they have more flexibility. However, price fluctuations in the intraday market are harder to predict leading to more difficulties in planning this kind of arbitrage.

Balancing market
The shortest term market is the balancing market, operating within one PTU before energy needs to be delivered. The short time span on which this market operates makes it the most volatile of all available markets with very large, albeit not many, price spikes. These price spikes can be used if the utilized storage technique is capable of responding quickly. DNV-GL concludes that the frequency and amplitude of spikes on the balancing market will decrease. This is caused by better prediction techniques and more international connections to absorb intermittent effects.

2.4.2 Flexibilty and ancillary services

The report by DNV-GL has outlined the flexibility services which need to be performed along with the typical responsible party, current measures, time scale, power level and energy quantity in 2.8 (Dutch). In the table the abbreviations TSO and DSO stand for Transmission System Operator and Distribution System Operator respectively and TenneT is the TSO for the Netherlands.

Several categories of flexibility services can be identified. The top two rows outline services associated with power quality control and are characterized by short response times, low to moderate power and small to moderate energy quantities. These processes are operated almost continuously to ensure constant power quality.

The next three rows are concerned with balancing, reserve and emergency power. When the power committed to producing power and consuming power do not match at any given moment, the TSO contracts more consumers or suppliers to balance the load. The time scale at which these suppliers or consumers can react to the request of the TSO determines for which of the services they can be contracted. Also note that the minimum needed power for these three services is also

very high. This is caused by regulations stipulated by the TSO to limit the amount of providers of this service; making it easier manage the providers and to ensure that the providers are reliable.

The following two rows refer to congestion management in the transmission and distribution networks. Congestion occurs when the energy transfer desired by the market cannot be carried out due to limitations of the network. Currently short term congestion problems can be rerouted and systematic problems can be alleviated by reinforcing the network with more conductors. The amount of power and energy needed for this service are large in the transmission system and moderate in the distribution system. The time scales are moderate for both systems. Furthermore, due to the localized nature of congestion problems distributed congestion alleviation is preferred over centralized options.

Currently these flexibility services are performed by large consumers and producers of energy by fluctuating their produced or consumed power. Emergency power is supplied by contracted suppliers often times in possession of emergency generators. These suppliers need to be able to provide large amounts of power (20 MW) and face large penalties when they cannot supply. Such contracts for congestion services do not exist but they are expected to be developed to deal with increasing congestion. This congestion is expected to arise from large surpluses of renewable energy or synchronized demand spikes due to demand response. Congestion markets can take different forms such as variable electricity pricing to quell demand response spikes, direct control of demand response devices by the DSO or excess power absorption by electricity storage. What market eventually will developed is still unknown [4].

Functie	Verantwoordelijke partij	Huidige middelen	Relevante tijdsschaal	Relevante vermogensschaal (MW)	Energiebehoefte (ordegrootte)
Beheer van spanningskwaliteit	TSO/DSO	Wordt beperkt geregeld. (FACTS, filters, regeltransformatoren, blindvermogensinjecties)	0.01-1 sec	0.001-1	Klein
Spannings-/blindvermogenshuishouding	TSO/DSO	Regelvermogen, transformatortapstanden, regeltransformatoren, FACTS	1-1000 sec	0.01-10	< 1 MWh
Frequentieregeling	TSO	regelvermogen	0,1-100 sec.	1-1000	< 10 MWh
Balanshandhaving (<15 min.)	TSO	reservevermogen	15 min.	1-1000	0.1 - 100 MWh
Balanshandhaving (>15 min.)	TSO	noodvermogen	1-10 uur	10-1000	10 - 1000 MWh
Congestiemanagement, transmissie	TenneT	redispatch, netverzwaring	0.1-10 uur	10-1000	1-1000 MWh
Congestiemanagement, distributie	DSO's	netverzwaring	0.1-10 uur	0.1-10	0.1-10 MWh
Energiemanagement achter de meter	Consument	Niet / netverzwaring / salderen	0.1-10 uur	0.001-0.01	0.001-0.01 MWh
Ramp rate control	Producent	economische dispatch, unit commitment	0.01-1 uur	10-100	1-100 MWh
Economische inzet van centrales	Markt	economische dispatch, unit commitment	1-100 uur	10-1000	10-10.000 MWh
Onderhoudsplanning	Producent	individuele planning per bedrijf	10-1000 uur	100-1000	1-1000 GWh
Seizoensfluctuaties in vraag en aanbod opvangen	Op dit moment geen	wordt verzorgd door producenten	1000-10000 uur	100-1000	100 – 10.000 GWh

Figure 2.8: Overview of flexibility and capacity services with typical operating parameters [4]

2.4.3 Profitability and regulatory boundaries

A major issue affecting the wider implementation of electricity storage systems is the higher costs they add to the already expensive transmission and distribution networks or deployment of renewable energy systems. This often renders them uneconomical if used for a single application when compared with alternative conventional solutions.

Therefore it is important for incumbent technologies to be useful for multiple applications so that, if properly managed, multiple income streams can be generated. Technologies which are capable of offering several services combine instantaneous to fast response with moderate storage capacity or moderate response with large storage capacity. This allows the technologies to compete on both the flexibility and energy markets or the energy and capacity markets respectively.

For energy applications the main barriers are as follows. The predominant mechanism to profit from energy applications is through energy arbitrage. How much money can be made through this mechanism is directly dependent on the short term price difference between spot prices for electricity. These prices can be depressed by large bids from large suppliers. This makes it more difficult for small suppliers to correctly forecast prices [11]. Due to the European legislation forcing the electricity systems in member states to be unbundled difficulties arise when flexibility services are to be performed with electricity storage. Due to the nature of flexibility services it entails the buying and selling of electricity while strictly being a part of the distribution system. This results in the stacking of fees for suppliers and consumers and legal problems regarding supplying electricity whilst supporting the DSO.

For capacity applications TSOs dictate a minimum power capacity and operation time for capacity suppliers. This is done to limit the amount of suppliers and make it easier to guarantee reliability of supply. However, the powers demanded by the TSOs are in the order of megawatts which is not realistic for decentral storage applications. Until now these regulatory boundaries make it very hard for suppliers of storage capacity to enter the market. Industry parties are lobbying for these rules to be changed. However, whether or not these regulations will be changed is uncertain and lies outside the scope of this report.

2.4.4 Implications for the Ecovat system

From the report by DNV-GL it can be concluded that trading on the long term market proves most promising for storage times between 2-3 days. On these time scales relatively large price fluctuations up to 50-60 EUR/MWh are expected due to meteorological effects. Longer storage times do not seem profitable due to lower price differentials and the possibility for fewer charge/discharge cycles.

As mentioned before the balancing market provides the largest price differences. These are, however, by their nature not predictable and short lived. Therefore only very fast acting storage methods such as flywheels and batteries are feasible.

The main focus of the Ecovat electricity storage module is to form a complete energy storage system in combination with the usual heat storage unit. This system would allow the Ecovat system to manage the total energy supply of its connected consumers. By bundling the electricity demand of all the consumers it becomes possible to provide emergency power from storage in case of an outage, a service not yet provided in the current electricity market. The potential monetary value of such a service is unknown and has not been investigated in a residential context. However with the increase of renewable energy sources in the energy mix the reliability of energy supply might deteriorate, and more self-sustaining local grids might be desirable. Furthermore, due to the expected increase in installed solar PV capacity in the residential sector, local storage of electricity will prove more profitable and maybe even essential for distribution grid stability.

2.5 Heat storage for electricity generation

As mentioned in the introduction, this thesis particularity focuses on electricity storage by storing it in the form of high temperature heat. In the next section some background information about converting electricity to heat and vice versa is provided. After which, this information can be combined with the previous sections to determine possible storage configurations.

Heat can be converted into electricity by the use of heat engines, such as steam turbines, in combination with a generator. The maximum efficiency with which thermal energy can be converted into electricity is directly dependent on the temperature difference driving the heat engine. In practice this means that higher input temperature leads to greater conversion efficiency. Electricity production from heat storage is therefore mostly applied in contexts where high temperature heat is readily available, such as concentrated solar power (CSP) plants. CSP plants reach temperatures of several hundred degrees centigrade, and can therefore convert the heat to electricity with reasonable efficiency.

The Ecovat system does not produce such high temperatures so these would have to be produced using electric heaters. However, HTS has a possible synergy with the Ecovat system. One of the drawbacks of HTS is high energy losses to the ambient due to an increased temperature differential. By placing the storage within the Ecovat vessel the temperature gradient could be diminished and any remaining losses would be absorbed by the low temperature vessel. This means that the cooling of the HTS would only lead to a loss of exergy and not a loss of energy. Because of this reason HTS is considered as a possible means for electricity storage in the Ecovat concept.

Another option is to use technologies currently implemented in waste heat to electricity conversion processes. These processes operate at lower temperatures which would make the energy easier to store whilst maintaining efficiency. These processes do require more capital investments per kW installed and are harder to scale than high temperature installations.

In any case the HTS system will consist of a storage module and two conversion modules, from electricity to heat and vice versa. Technical possibilities for each of the conversion steps are discussed below. The information used in the next section regarding storage principles is taken from two studies outlining the state of the art in HTS [8] [13].

2.5.1 Power to heat

Heat pumps are used to maximize the efficiency of the conversion from electricity to heat while charging the water vessel. The temperatures needed for HTS cannot be achieved with heat pumps. Electric heaters can reach these temperatures and depending on the configuration electric boilers or immersion heating elements are preferred.

2.5.2 Heat to power

As mentioned before conversion from heat to power is usually done by connecting a heat engine to a generator. The predominantly used heat engine is a steam turbine which is the preferred heat engine for conventional fuels such as coal. To prevent nucleation of the water inside the turbine whilst having sufficient expansion over the turbine, the inlet temperatures and pressures needed for steam turbines are quite high. These temperatures can routinely be reached using fossil fuels sources but are harder to achieve using renewable energy sources.

To convert heat from lower temperature sources into electricity an Organic Rankine Cycle (ORC) can be used. ORCs operate on the same principle as the steam turbines, i.e. the Rankine cycle, but do not use water as the working fluid. By using another working fluid, such as CO2 which has a different saturation curve, higher efficiencies can be achieved whilst using lower operating

temperatures. ORC generators are currently used to utilize lower temperature heat sources such as geothermal heat or waste heat sources. A third possible heat engine is the Stirling engine. This technology can reach high efficiencies at low temperatures and can use heat from a large variety of sources. This makes the Stirling engine especially suited for waste heat sources, and the technology has seen a surge in interest as the demand for energy saving measures increases. The applications have however been limited to relatively small scale installations due to difficulties with scaling the technology.

2.5.3 Sensible heat storage

Sensible heat storage refers to storing the thermal energy in a material which increases in temperature as it is charged. Many different heat storage techniques and materials are used for sensible heat storage. The three most commonly used material categories are molten salts, thermal oils and concretes. The general attributes of these three categories are elaborated upon below but within these categories large variations may occur for specific materials.

Storage techniques can be divided into several categories, the largest of which are active and passive storage. Active heat storage means that the storage material itself is pumped through a heat exchanger during charging and discharge. Passive storage indicates that a heat exchanger which charges the storage is placed in the storage material and the storage is charged by running a heat transfer fluid (HTF) through the heat exchanger. Active storage can be subdivided into direct and indirect storage. This distinction refers to whether the heat storage material is also the HTF (direct) or that another HTF is used to transport the heat from the source to the storage (indirect).

Molten salts have been popular as a heat storage material due to fact that they are liquid at atmospheric pressure when heated to high temperatures, have good heat capacity and thermal conduction and can be relatively cheap. Furthermore, molten salts are compatible with the operating requirements of steam turbines. One major drawback of using molten salts is their high freezing temperature. One of the most used commercial salts freezes at 224 degrees centigrade. Therefore the storage and any pipes containing the salt must be kept at high temperatures to avoid solidification. Furthermore, the high temperatures needed for storage lead to higher losses during operation.

Mineral and synthetic oils do not freeze at lower temperatures but also lack some of the beneficial attributes of molten salts. They have lower thermal conductivity and volumetric specific heat capacity leading to larger storage requirements and lower charge and discharge rates. Furthermore, thermal oils need to be pressurized to reach the same temperatures as molten salts. The cost of thermal oils varies greatly with composition and can be very high. Some of these costs might be mitigated by using mixed medium tanks to lower the amount of oil needed.

Other novel approaches to single tank HTS aimed at improving stratification or reducing costs are floating stratification barriers and immersed steam generators [3].

Concrete is a promising heat storage material due to its low price, good thermal conductivity and abundance of materials. Because concrete is a solid only passive storage is possible and therefore heat exchangers need to be integrated in the storage material.
In the next chapter the findings regarding the electricity markets and conversion technologies are applied to the Ecovat context.

Chapter 3

Electricity storage in the Ecovat context

In the previous chapter the changing markets for electricity storage have been discussed along with possible revenue generating configurations. Due to the goal of this thesis to implement the electricity storage module in the existing Ecovat system, the typical parameters of this system should be taken into account. This chapter discusses the parameters of the Ecovat system, its typical clients and what these parameters mean for the electricity storage module and conversion module.

3.1 Typical clients

The Ecovat energy storage system is a large scale sensible thermal energy storage module meant for seasonal heat storage. When storing energy in the form of sensible heat, large scale storage modules are preferred over smaller ones. This is due to the fact that the energy storage capacity scales with the volume of the storage unit and the losses scale with the outer surface area of the module. However, when larger storage modules are used, more consumers are connected to one storage site. This increases the average distance between storage and consumer, and consequently transport losses increase. Therefore, the advantages of large scale storage need to be balanced with additional transportation losses caused by more spread out customers. These factors limit the applications for which an Ecovat of a particular size is suitable, and therefore Ecovat focuses on three distinct market sectors. These sectors are: the built environment, greenhouse food production and heat grids. In all of these application the Ecovat system which is implemented is roughly the same, but some details differ between the applications.

The built environment sector refers to larger scale housing projects with one contracted heat supplier. This means that all the heat demands of the entire housing project are met by one supplier, allowing the investment in a shared large scale storage such as an Ecovat. Examples of these are large apartment complexes, campuses of different kinds and public housing projects.

Greenhouse agriculture requires a large amount of heat to make sure the crops can still be grown during the winter. Due to the large heating demand one greenhouse farmer has, an Ecovat system can prove profitable when connected to a single consumer.

The last sector is district heating networks connected to a heat source, for example waste heat or geothermal heat. The advantage of installing an Ecovat system in the heating network is that more consumers can be connected to the same heat source. Due to load shifting the peak heating production required during winter is lowered, allowing for a more stable production profile and more connected consumers.

3.2 Storage size and power requirements

As discussed in the previous chapter to achieve a positive business case with electricity storage the stacking of services is crucial. Therefore the storage system should be dimensioned in such a way that multiple services can be performed by the same system. This means for example that power delivery capacity might be over dimensioned for pure arbitrage services to also allow for balancing services. Furthermore, due to the fact that Ecovat is already engaged in heat storage and supply services for its clients, integration of electricity storage services would result in a complete energy supply service for its connected consumers. However, providing this service demands different design parameters than both arbitrage and services.

In the following section the technical parameters associated with these different services are discussed. This is done to determine what specifications the electricity storage module should have to serve its intended use. The application used to preform this analysis is the scenario where the Ecovat is used in the built environment, serving a number of contracted consumers. The Ecovat system provides heating and backup power for these consumers with the possibility of performing arbitrage and flexibility services.

3.2.1 Backup power

The thermal storage capacity of the Ecovat systems go up to 4.5 MWh of thermal energy to be used for space heating and hot water supply. On an annual basis a storage of this size is able to provide heat storage services for around 300 dutch households. The aim of the electricity storage unit is to be able to provide two days of emergency electricity for its connected consumers. The average annual electricity consumption of one dutch household is 3500 kWh. The energy needed to provide 300 households with electricity for up to two days is therefore approximately 5750 kWh, not accounting for storage and conversion losses. The power consumed by a typical Dutch household peaks at just below 1 kW for terraced housing connected to district heating systems [10]. The total electric power output of the system should therefore be at least 300 kW to meet the peak demands of the connected consumers.

3.2.2 Flexibility services

The relevant power, storage capacity and timescales required by different flexibility and capacity services differ greatly between services. The parameters required for these services should by comparable to the parameters needed for backup power, to efficiently incorporate the flexibility services in the electricity storage system. An overview of these parameters is given in figure 2.8.

The power and energy storage parameters for backup power, 300 kW and 5750 kWh, align best with the parameters of: voltage control, congestion management in the distribution grid and consumer energy management. Whether the response time of the energy storage module is suited for voltage control is unlikely. This is due to the fact that to preform voltage control services very fast reaction times are required, i.e. within one second. Techniques capable of reacting that quickly, for example flywheels, do not have significant storage capacity and are therefore not suited for electricity storage purposes. These techniques are therefore not considered for the electricity storage module, and voltage control services can consequently likely not be performed.

The one MW minimum power requirement for many of the flexibility services is currently dictated by the regulatory framework stipulated by the TSO 'TenneT'. This is done to limit the number of suppliers able to participate in this market, which makes it easier for the TSO to manage the reliability of its flexibility service providers. A different regulation requires the balancing service providers to balance their energy ledgers. This means that on a daily basis each provider is required to conform to their pledged net consumption or production of electricity, or else endure a fine. These regulations make it harder for energy suppliers with limited power and energy

management capabilities to enter the flexibility market. It has been proposed to remove one or both of these regulations, which would open up the possibility for more players, such as Ecovat, to offer flexibility services. This lifting of regulations could help shift the flexibility services away from the fossil fuel power plants, towards smaller more sustainable providers. However, because of the uncertainty regarding these regulatory changes, one cannot assume these services will provide a reliable source of revenue. Therefore the design of the system is not altered to accommodate the performance of these services.

In the case that the balancing requirement but not the power requirement is lifted, the Ecovat system could preform balancing services by consuming more power to convert to heat. In the case that both regulations are lifted electricity could be supplied back to the grid from the electricity storage. However, whether this makes economic sense is strongly dependent on the balancing tariff offered by the TSO. This is due to the conversion losses associated with storing the energy. The value of the lost energy needs to be compensated by the difference between tariffs charged for consuming and supplying the energy. On the balancing market the tariff is dictated by how much the realized supply and demand of electricity differs from the planned supply and demand. These tariffs can make the price of electricity skyrocket when consuming at the time of a shortage. On the other hand the price of energy can also become less then zero when there is an excess of energy. The tariffs are determined in time slots of 15 minutes. An estimation of how many time slots were profitable in the previous year, for either buying or selling at different conversion efficiencies, has been conducted. The results of these estimations suggest that only a very limited number of time slots would prove profitable. Therefore it is not likely that the electricity storage would be used for balancing services in the scenario that the TSO demands balancing of the energy ledger.

3.3 Conversion methods

To store electricity in the form of heat the energy needs to be converted from electricity to heat and back. To preform these conversions several technologies exist. The conversion from power to heat can be done using resistive heating at an efficiency approaching 100 %. Using heat pumps even higher conversion efficiencies can be achieved. However, the output temperatures of such heat pumps are limited. The conversion from heat to power is usually done by connecting a heat engine to a generator. Several heat engines can be used for this step, three of these are discussed below. In the next subsections these three technologies will be compared with respect to their efficiency, price and practical applicability in the Ecovat setup.

The predominantly used heat engine is a steam turbine which is the preferred heat engine for conventional fuels such as coal. Steam turbines have high efficiency at high temperatures and can be used at large scale. To prevent nucleation of the water inside the turbine whilst having sufficient expansion over the turbine, the inlet temperatures and pressures needed for steam turbines are quite high. These temperatures can routinely be reached using fossil fuels sources but are harder to achieve using renewable energy sources.

To convert heat from lower temperature sources into electricity an Organic Rankine Cycle (ORC) can be used. ORC's operate on the same principle as the steam turbines, i.e. the Rankine cycle, but do not use water as the working fluid. By using another working fluid, such as CO_2 which has a different saturation curve, higher efficiencies can be achieved whilst using lower operating temperatures. ORC generators are currently used to utilize lower temperature heat sources such as geothermal heat or waste heat sources. Depending on the application in which the ORC is used, the mode of operation (subcritical, transcritical) and the working fluid can be varied to optimize the conversion efficiency and limit component sizes.

A third possible heat engine for this application is the Stirling engine. This technology can reach high efficiencies at low temperatures and can use heat from a large variety or sources. This makes

the Stirling engine especially suited for waste heat sources, and the technology has seen a surge in interest as the demand for energy saving measures increases. The applications have however been limited to relatively small scale installations due to difficulties with scaling the technology.

3.3.1 Efficiency

The efficiency of all three conversion technologies is dependent upon the inlet temperature of the heat engine, with higher inlet temperatures leading to higher efficiencies. The maximum efficiency which can be achieved at a certain inlet and outlet temperature is dictated by the Carnot efficiency. This efficiency holds true for all heat engines and is defined as follows:

$$\eta_{carnot} = \frac{T_{max} - T_{min}}{T_{max}} \tag{3.1}$$

For efficient energy storage it is beneficial to store the energy at a low temperature. The ideal conversion method therefore has the highest efficiency whilst limiting the storage temperature.

Steam turbines
Steam turbines which are used in electricity generation have a conversion efficiency typically of around 30%. However, these steam turbines are driven by fossil fuels such as coal which can reach very high temperatures which lead to high efficiencies. At lower temperatures the efficiency drops sharply. This is because at lower temperatures the pressure drop over the turbine which can be realized is limited due to the risk of nucleation. Nucleation occurs when a superheated vapor is cooled down, or expanded to the point where the superheated vapor becomes a saturated vapor. The limited pressure drop over the turbine limits the work which can be extracted by the turbine limiting the overall efficiency of the cycle.

ORC's
Some organic fluids are so called dry fluids, which means that when expanded over a turbine they do not become a saturated vapor without substantial heat extraction. This means that no nucleation will occur even at lower operational temperatures. Due to this attribute these kinds of fluids are referred to as 'dry fluids'. Dry fluids allow for a larger pressure difference between the inlet and the outlet of the turbine which leads to more work extraction. This is the main advantage of using organic working fluids in Rankine cycles, which leads to higher conversion efficiency at low temperatures. What efficiency can be achieved differs greatly per working fluid and specific ORC design, this will be elaborated upon in the ORC fluid section.

In figure 3.1 a T-s diagram containing the saturation curve of an organic dry fluid is shown, with an example of a Rankine cycle superimposed onto it. In the figure it can be seen that during the expansion over the turbine, from point 4 to point 5, point 5 cannot end up within the vapor curve without decreasing the specific entropy. The specific entropy cannot decrease until heat is extracted from the fluid. This is done when the fluid has exited the turbine into the condenser.

Stirling Engines
Stirling engines are not a common method for converting heat to work in power generation applications. However due to the increasing demand for ways to convert waste heat into electricity research into Stirling engines has seen a resurgence in recent years. Especially in the field of concentrated solar thermal power the installation of Stirling engines on dish style concentrators has proved promising. These applications are however small scale partly due to the fact that Stirling engines require a lot of raw material. They are however easy to operate and require little maintenance. One of the largest Stirling engines in production is Coolenergy's ThermoHeart Stirling engine. The ThermoHeart has a rated power of 25 kW at a supply temperature of 400 degrees centigrade, multiple engines can be connected in parallel to achieve higher power capabilities. According to the manufacturer efficiencies of up to 30 % can be achieved. These claims are however

not verified by third parties, and due to the limited implication of the technology little experience with the product is scarce.

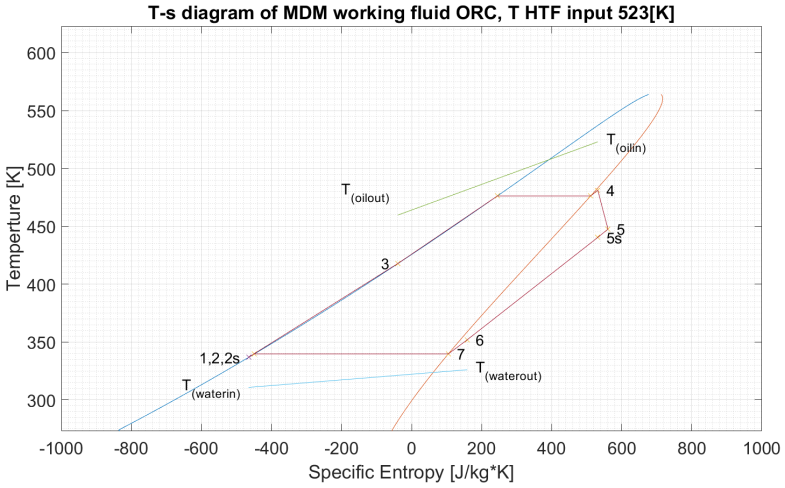

Figure 3.1: Example of a T-s diagram for an ORC

3.3.2 Price per kW installed capacity

To estimate the costs associated with each of the conversion technologies the costs per kW installed capacity are considered. This approach does not take into account the operational costs, but does provide an accurate approximation for the initial investment costs.

The installation cost of steam turbine units listed in literature mostly focuses on the widely implemented large scale steam turbines. These are however not representative for more small scale units where the price per kW tends to be higher. For midscale systems in the range of a few hundred kW the price per kW installed is around 1000 $ per kW.

For ORC system the application in which the system is used and the scale of the system greatly influence the price per kW installed. Depending on the application some components in the ORC system can be completely omitted, for example CHP installations need a boiler vessel whilst waste heat applications do not. The application within the Ecovat system, where heat is taken from a storage vessel, resembles the waste heat recovery applications the most. Therefore it is assumed that the price for waste heat recovery modules is comparable to the Ecovat application. The price trends of different ORC systems of different sizes is shown in 3.2. From this figure it can be seen that waste heat recovery (WHR) applications, in the range of a few hundred kW, typically cost around 1500 $ per kW installed.

The number of commercially available Stirling engines of considerable size are limited, so a representative price point is hard to establish. The one Stirling engine of sufficient size that was found, Coolenergy's ThermoHeart, sells for between 45000 and 50000 $. This places the price per kW installed for this specific Stirling engine at around 2000$.

3.3.3 Practicality

Even though the operating principles of steam cycles and organic Rankine cycles are very similar there are some differences regarding practicality in specific applications. In the next section the advantages and disadvantages of both technologies are discussed.

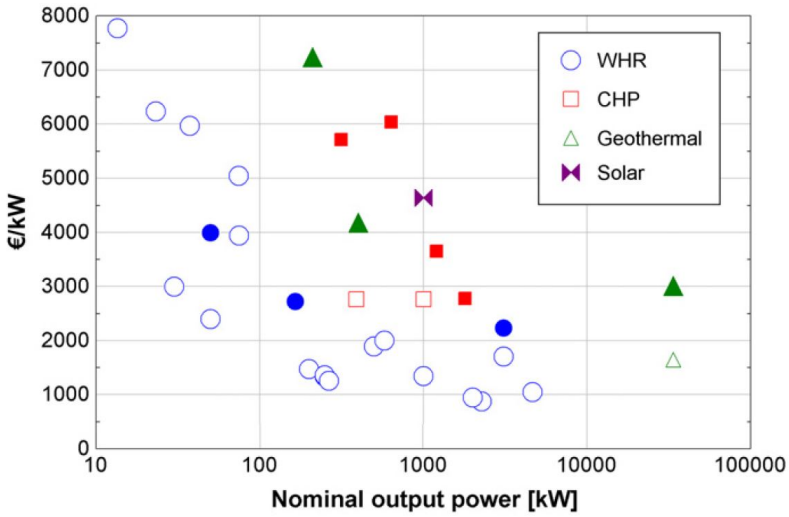

Figure 3.2: Overview of ORC module prices[18]

The use of organic working fluids allows for lower operating temperatures then with steam cycles. This removes the necessity for superheating of the working fluid which simplifies the heat exchanger design. Furthermore, due to the fact that the inlet temperature is less of a constraint for ORC's, the heat storage can be depleted further without significant risk. The other main advantage over conventional Rankine cycles is that ORC's are smaller and less complex to build. This has two main causes, firstly the density of the operating fluid is higher and secondly the operating pressures are lower. Due to the higher density of the working fluid the total volume flow through the system is smaller directly decreasing the size of the components. The lower operating pressure decreases the pressures the system should be able to withstand and decreases the turbine blade speed allowing for simpler turbine design. The lower complexity of the system allows the ORC to be operated without supervision and with a simple startup sequence.

The advantages of the steam cycle are that the working fluid is cheap and abundant. Furthermore, the lower density which increased the needed volume flow does decrease the pumping power needed leading to lower parasitic losses.

Overall the ease of operation and high efficiency at lower temperatures of the ORC has made it the preferred choice for the Ecovat electricity storage system. The higher costs associated with the ORC in comparison with ordinary Rankine cycles are compensated by the efficiency of the conversion process. This is due to the fact that higher conversion efficiencies decrease the amount of energy that needs to be bought and stored. Furthermore the larger temperature range allows for a smaller amount of storage material further decreasing the total cost of the system. This will be elaborated more upon in the following section concerning the storage module.

3.4 Storage Module

The storage module in a sensible heat storage system consists of a material in which to store the heat and a heat exchanging surface to transport the heat into and out of the medium. In the following section the materials which can be used are compared, the dimensions of the system are considered and the costs of the entire module are estimated. At the end of this section the heat storage medium for the Ecovat electricity storage system is decided upon.

3.4.1 Materials

For sensible heat storage numerous different storage materials exist, each with distinct characteristics. These determine for what applications the materials are suited. The optimal storage module has a high storage density, can be operated at the desired temperature, needs little heat exchanger surface area and uses inexpensive, non toxic materials. Not all of these attributes can be achieved simultaneously. Therefore the total costs needed to construct a storage module with each of the materials are computed. The results from these calculations are used to select the cheapest options. These options are then compared with respect to their practicality to determine the most feasible option. The materials which are considered in this analysis are listed in 3.3 along with their relevant characteristics. The conversion techniques considered in the previous

Table 1
Main characteristics of sensible heat storage solid materials [4,10].

Storage medium	Temperature		Average density (kg/m^3)	Average heat conductivity (W/m K)	Average heat capacity (kJ/kg K)	Volume specific heat capacity (kWh_t/m^3)	Media costs per kg (US$/$kWh_t$)	Media costs per kWh_t (US$/$kWh_t$)
	Cold (°C)	Hot (°C)						
Sand-rock-mineral oil	200	300	1700	1.0	1.30	60	0.15	4.2
Reinforced concrete	200	400	2200	1.5	0.85	100	0.05	1.0
NaCl (solid)	200	500	2160	7.0	0.85	150	0.15	1.5
Cast iron	200	400	7200	37.0	0.56	160	1.00	32.0
Cast steel	200	700	7800	40.0	0.60	450	5.00	60.0
Silica fire bricks	200	700	1820	1.5	1.00	150	1.00	7.0
Magnesia fire bricks	200	1200	3000	5.0	1.15	600	2.00	6.0

Table 4
Main characteristics of sensible heat storage liquid materials [10,12].

Storage medium	Temperature		Average density (kg/m^3)	Average thermal conductivity (W/m K)	Average heat capacity (kJ/kg K)	Volume specific heat capacity (kWh_t/m^3)	Media costs per kg (US$/$kWh_t$)	Media costs per kWh_t (US$/$kWh_t$)
	Cold (°C)	Hot (°C)						
HITEC solar salt	120	133	–	–	–	–	–	–
Mineral oil	200	300	770	0.12	2.6	55	0.30	4.2
Synthetic oil	250	350	900	0.11	2.3	57	3.00	43.0
Silicone oil	300	400	900	0.10	2.1	52	5.00	80.0
Nitrite salts	250	450	1825	0.57	1.5	152	1.00	12.0
Nitrate salts	265	565	1870	0.52	1.6	250	0.50	3.7
Carbonate salts	450	850	2100	2.0	1.8	430	2.40	11.0
Liquid sodium	270	530	850	71.0	1.3	80	2.00	21.0

Figure 3.3: Considered storage materials with properties [8]

section do not operate in the same temperature range, and have different conversion efficiencies. Therefore the amount of storage material needed to store the same amount of energy differs per conversion technology. This is accounted for in the calculation. Only the part of the material's operating range which overlaps with that of the conversion technology, is counted towards the storage capacity. For example, the operating range of the Stirling engine is between 150 and 400 degrees centigrade. Therefore if the heating range of a material extends below 150 degrees this part of the temperature range is disregarded. If a combination of storage material and conversion technology has no overlap, it is not considered. This becomes especially important when considering the molten salt storage materials. These materials solidify at high temperatures which may cause them to solidify during discharge. Solidification of the storage material is not desired as it lowers the discharge power available and may lead to 'dead' regions within the storage material which cannot be used. For example the carbonate salt materials solidify at 450 degrees centigrade. Any conversion method operating under this level cannot be used in conjunction with this material. The volume of the storage material needed to store the needed thermal energy is shown in 3.4. Which storage material refers to which bar in the graph is listed in the following overview.

Heat exchanger surface area
The amount of heat exchanger surface area needed to extract the energy from the storage module is also material dependent. The variable which determines the needed heat exchanger area, for stagnant storage materials, is the thermal diffusivity α. Thermal diffusivity is the combination of three other material characteristics: thermal conductivity, density and specific heat capacity. These three variables influence how quickly the heat is transported through the material, and the length the energy needs to be transported through the material. If thermal diffusivity is lower

1	Mineral oil
2	Synthetic oil
3	Silicone oil
4	Sand rock mineral oil
5	Reinforced concrete
6	Solid NaCl
7	Cast iron
8	Cast steel
9	Silica fire bricks
10	Magnesia fire bricks

Table 3.1: Considered storage materials

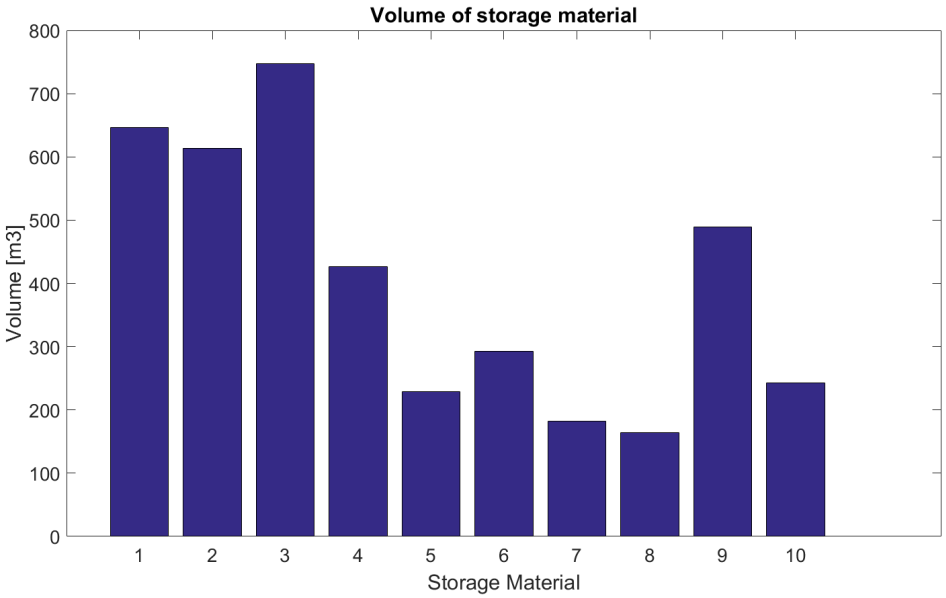

Figure 3.4: Storage volume needed for the different storage materials, ORC

more heat exchanger area is needed to achieve the same thermal power. To determine how this parameter influences the are of the heat exchanger the following calculation is carried out. We assume that the heat exchanger consists of cylindrical pipes with a length of 20 meters, surrounded by the heat storage material. The radius of heat storage material surrounding the pipe is defined as: the maximum radius that still allows the required power to be extracted, given a temperature difference of 10 degrees between the steel pipe and the outside of the storage material. The number of pipes is then calculated by dividing the total storage volume by the amount of storage material surrounding one pipe. This indication of the amount of heat exchanger material needed for each of th storage materials is used in the module cost calculation.

3.4.2 Cost of storage module

By combining the costs of the heat exchanger and the storage material the costs of the total module can be estimated. This is done for the considered materials when used in conjunction with an ORC conversion module operating between 150 and 300 degrees centigrade. The costs of the conversion module are also present in the total. One of the materials is omitted from the graph because the costs were so high that the graph would distort when they were included.

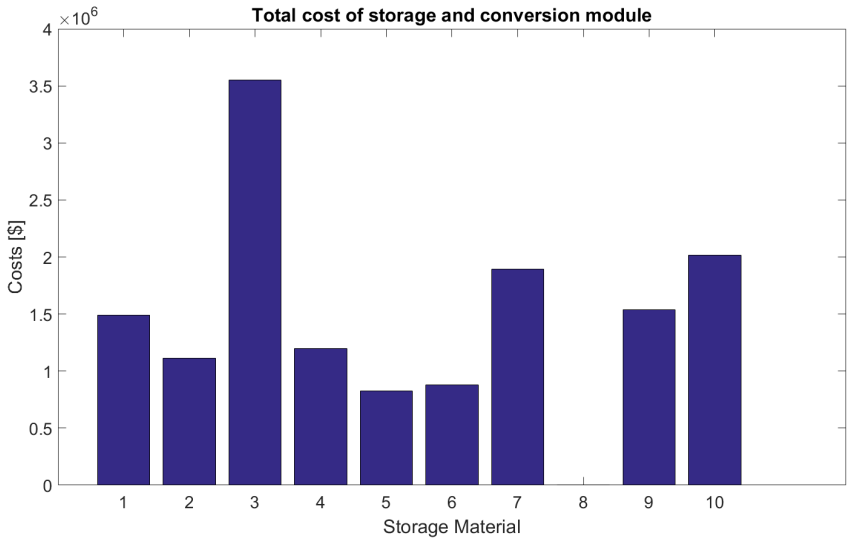

Figure 3.5: Cost of storage material, heat exchanger and conversion module

From 3.5 it can be seen that the total storage module costs are lowest when using reinforced concrete (5) or solid NaCl (6).

3.5 General module design

An inherent problem of storing energy in the form of heat are losses to the environment. By integrating the high temperature storage inside a low temperature energy storage some of these losses might be mitigated. Furthermore, any losses from the high temperature storage which do occur are absorbed by the low temperature storage. This diminishes the cost of the lost energy as it can still be extracted as low grade heat. To achieve this the high temperature storage needs to be situated inside the low temperature storage vessel. To allow this the overall size of the storage needs to be limited. The volume of the storage module differs per material as the storage density and operational temperature range differs per storage material. Influencing the minimal size of the module.

Besides the requirement that the storage module can be integrated in an Ecovat system, the placement within the system is relevant as well. The high temperature storage module is preferably confined to the upper region of the tank. This is done to minimize interference with the existing stratification present inside the tanks. Creating a storage module which extends deep into the tank causes the hot storage vessel to be located in colder regions of the tank. Furthermore, the long vertical wall of the storage could cause strong convective flows along the storage module. These convective flows could mix the storage vessel destroying any achieved stratification.

The goal of confining the vessel in the upper parts of the tank does interfere with decreasing the surface area of the storage. Creating a large flat storage module in the top of the tank would create a larger surface area for the same storage volume. How these conflicting design principles relate to each other needs to be investigated more before a conclusive answer can be given. In this report the storage module is modeled in segments and therefore the final geometry of the module is not necessary to carry out the simulations. For this report it is assumed the storage module consists of steel tubes of 20 meters surrounded by the storage material. How the arrangement of these tubes influences the system design is not studied in this report.

3.5.1 ORC working fluid selection and temperature range

Within the industry of ORC's several working fluids are used, depending on the application. The selection of which working fluid performs best in which circumstances has been studied extensively [7][9][20]. Comparing all the different possible working fluids lies beyond the scope of this report, but one needs to be selected nonetheless. To determine which working fluid to use a mix of academic papers and industry information was used. These sources were used to assess what is commercially available and what academic sources could be used for model validation.

In contrast with conventional Rankine cycles where water vapor is the default working fluid, ORCs can utilize a variety of different working fluids. These working fluids differ greatly in characteristics such as evaporating temperature, critical temperature, condensing behavior etc. Therefore, which working fluid is most suited depends greatly on its application. For the specific Ecovat application the main purpose is to generate electricity with high efficiency and over a large temperature range to minimize the storage size. The conversion efficiency of an ORC, as with any heat engine, has on upper limit set by the Carnot efficiency. The Carnot efficiency increases as the temperature difference between the hot and cold heat flows in the cycle increases. As the cold temperature which can be reached in the cycle is limited by the ambient temperature, increasing the hot temperature is the most effective way to increase cycle efficiency. Therefore a working fluid with a high critical temperature is desired.

In an effort to determine which high temperature working fluid is most suited for the Ecovat application, industrial specifications of ORC generators operating in the relevant power range are consulted. Several manufacturers supply ORC generator units capable of supplying the 300 kW needed for the Ecovat application, i.e. Viking heat engines, Turboden, Adoratec and Siemens. These manufacturers focus on different temperature levels for their heat source and state different achievable efficiencies. Because high conversion efficiency is the primary performance indicator of the ORC in the Ecovat system, the manufacturer stating the highest rated performance, Siemens, is chosen as a starting point for the ORC design. The Siemens system operates with an input temperature of 300 degrees centigrade and reports a thermal conversion efficiency of 18%, other manufacturers such as Adoratec report similar figures but supply less details about the installation.

The data sheet of the Siemens system does not state the working fluid used in the cycle [19]. However, due to the known temperature range of the cycle and with the description of the working fluid which was, given it is plausible that the working fluid is a siloxane or more commonly referred to as a silicone oil. These compounds have a number of desirable characteristics for ORC's such as low toxicity and flammability, good thermal stability and good material compatibility [7]. The performance of several of these siloxane compounds has been studied for use in ORC applications. A short overview of these fluids and their characteristics is given in figure 3.6. The fluid octamethyltrisiloxane, also known as MDM, was selected as the working fluid for this model as it is a widely used siloxane in ORC optimization studies, this allows the model to be accurately compared with other models such as those listed in [7], [12], [15], [17].

Once a suitable working fluid is selected the specific cycle and component parameters need to defined. In its most basic form an ORC consists of four components: pump, heater, expander and condenser. This basic principle of the cycle is present in all ORC's but adjustments to operating temperatures can be made. The main adjustments which can made to operating temperature are whether the turbine inlet is superheated and or transcritical. When the inlet is superheated the working fluid is heated further after the working fluid has fully vaporized. Transcritical operation refers to heating the working fluid to above its critical temperature. Both these adjustments can be used to utilize heat sources with input temperatures higher than the desired evaporation temperatures. However, these modes of operation do put an extra strain on the system to withstand higher pressures and more complex heat exchanger and turbine design [12].

Thermodynamic characteristics of siloxanes.

Compound	Molecular Mass, M (kg/kmol)	Critical Pressure, p_c(bar)	Critical Temp., t_c(°C)	Boiling Temp., t_b(°C)	Acentric Factor
MM	162.37752	19.39	245.60	100.52	0.419
MDM	236.531	14.15	290.94	152.53	0.5297
MD_2M	310.685	12.27	326.25	194.35	0.668
D_4	296.61576	13.32	313.35	175.00	0.589
D_5	370.7697	11.60	346.00	210.95	0.6658
D_6	444.924	9.61	372.63	244.99	0.7361

Figure 3.6: Overview of working fluid characteristics used in [7]

Another adjustment which can be made to the cycle is whether or not to include a recuperator. This component recovers energy from the working fluid flow exiting the turbine and transfers it to the working fluid exiting the pump. A recuperator can improve the thermal efficiency of the cycle due to a better match between the T-s profile of the heat source and the working fluid. Therefore, recuperators are especially effective when the output temperature of the hot flow cannot drop below a certain level [12]

Whether such adjustments are beneficial depends on the combination of the working fluid and the heat supply profile. In the report of [12] a systematic optimization of ORC's with several working fluids and heat supply profiles was performed. In this analysis the optimal operating conditions of each working fluid were assessed. For the working fluid MDM the maximum input temperature was always below its critical temperature, therefore no supercritical heating was needed. When the output temperature was limited to a certain value the optimal solution contained a recuperator.

For the application within the Ecovat system the maximum input temperature can be controlled so transcritical operation is not needed. Furthermore the HTF is continuously cycled between the storage and conversion modules. Therefore, to limit the needed heat exchanging surface inside the storage material, the implementation of a recuperator is preferable. An example of such a cycle with an incorporated recuperator is show in figure 3.1.

How the performance of the conversion module described in this chapter and its interaction with the storage module is modeled in the following chapter.

Chapter 4

Mathematical model

In this chapter the mathematical model used to determine the performance of the proposed electricity storage system is formulated and verified. The storage system consists of the storage and conversion modules, which are modeled separately. In the last section of this chapter, these two models are linked to achieve a model for the complete system.

4.1 Organic Rankine Cycle

In the previous chapter the selection process for the working fluid and the mode of operation of the ORC are addressed. The following section expands upon the design parameters of the ORC and how the operating points and efficiency of the cycle are determined.

4.1.1 Design parameters

The goal of this mathematical model is to arrive at an ORC configuration to be implemented in an actual Ecovat storage configuration. Therefore design parameters are implemented to ensure technical and economical feasibility of the final cycle. These design parameters ensure that components do not become unfeasibly large or are exposed to unbearable stresses. These design parameters are used throughout the coming sections and are summarized here. The parameters are taken from a report by Maraver et al. which studied the optimization of ORC's whilst under environmental constraints [12].

Variable	Range/Value	Motivation
T_{pinch}	10 [K]	Limit size of heat exchanger
T_{sh}	5 [K]	Ensure full vaporization of working fluid
T_{sc}	5 [K]	Ensure full condensation of working fluid
P_{crit}	1.27e6 [Pa]	Working fluid may not exceed critical pressure
T_{crit}	557 [K]	Working fluid may not exceed critical temperature
ϵ_{IHE}	0.8 [-]	Effectiveness of the internal heat exchanger
SP	0.02 - 1 [m]	Characteristic turbine size limit

Table 4.1: Design parameters to determine operating points taken from Maraver

4.1.2 Determining operating points

The operating points of the cycle are dependent on the available input temperature of the HTF, therefore they need to be reevaluated during the discharge process. This input temperature is either a prescribed fixed value, or the output of the mathematical model of the storage module. In any case this value is known and can be used to determine the operational points of the cycle. Other fixed working points can be deduced from the dictated condensation pressure, super-heating and super-cooling temperatures. How the operational points are determined is outlined in the following section. The thermodynamic properties of the working and heat transfer fluids are taken from the CoolProp fluid library [2].

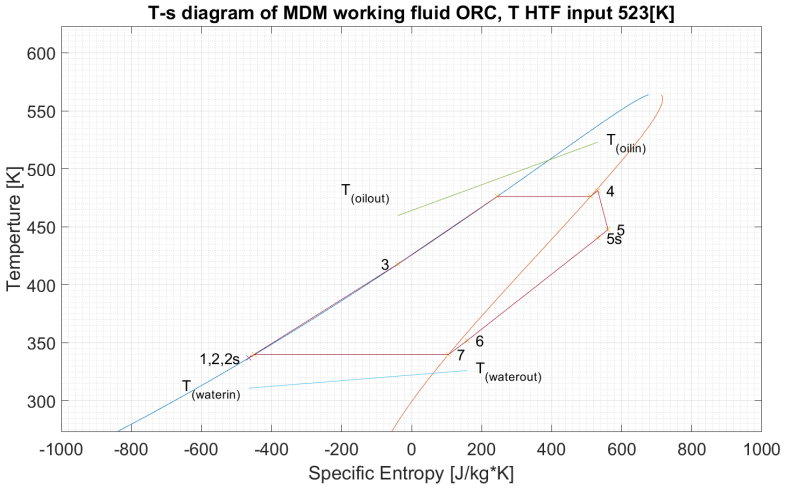

Figure 4.1: Example of a T-s diagram for an ORC

The pressure inside the condenser is set to 5 kPa in accordance with literature. This allows the condensation temperature T_7 to be defined as the condensation temperature of the working fluid at that pressure. The inlet temperature of the pump T_1 is equal to the condensation temperature minus the super cooling temperature T_{sc}. The temperature increase inside the pump is derived from the isentropic efficiency of the pump. Firstly the specific enthalpy and entropy in state 1, h_1 and s_1 respectively, are determined by using the CoolProp database. The enthalpy after isentropic compression, h_{2s}, is found by looking up the enthalpy of the working fluid under evaporator pressure whilst having the same entropy as operating point 1. When h_1, h_{2s} and the isentropic pump efficiency η_{ps} are known the enthalpy in point two, h_2, is calculated thusly.

$$h_2 = h_1 + \frac{h_{2s} - h_1}{\eta_{ps}} \tag{4.1}$$

After h_2 is assessed T_2 can be determined which serves as an input for further calculations.

From literature it was found that optimal exergetic efficiency was achieved when the slope of the heat source fluid temperature, closely matches the slope of the working fluid in the evaporator. To achieve this, whilst adhering to the boundary conditions for efficiency and heat exchanger effectiveness, the remaining operating points are determined using an iterative approach.

Firstly an arbitrary starting value for the evaporation temperature is chosen. This temperature is used to determine the exit temperature of the evaporator T_4. T_5, the output temperature of the turbine, is determined using a similar approach as for determining operating point h_2.η_{ts} represents the isentropic turbine efficiency.

$$h_5 = h_4 - \frac{h_4 - h_{5s}}{\eta_{ts}} \tag{4.2}$$

The inlet temperature of the evaporator, T_3 is dependent on the effectiveness of the recuperator,the input and output temperatures of the hot fluid T_5 and T_6. The mass flows for the cold and hot fluids within the recuperator are identical for they are both the mass flow of the working fluid. However, the heat capacity flow rate of the cold flow is higher than that of the hot flow due to lower specific heat of the working fluid at higher temperatures. This in combination with a heat exchanger effectiveness of less than 100 % places the pinch point of the recuperator at the cold side. This information leads to the conclusion that the inlet temperature of the condenser, T_6, can be determined by

$$T_6 = T_2 + T_{pinch}$$

Assuming a recuperator effectiveness ϵ_{IHE} the specific enthalpy, and consequently temperature, of operating point 3 are determined by

$$h_3 = h_2 + (h_6 - h_7) \cdot \epsilon_{IHE} \tag{4.3}$$

With all of the operating points of the working fluid known the operating points of the HTF and water flows are determined. As mentioned previously, to achieve the highest efficiency the temperature slope of the heat transfer fluid is matched to that of the working fluid inside the evaporator. Therefore, the temperature difference between the inlet and outlet of the heating fluid equals the temperature difference between working points 3 and 4. This results in the following expression for the output temperature of the heat transfer fluid.

$$T_{HTFout} = T_{HTFin} - (T_4 - T_3) \tag{4.4}$$

Because the evaporator temperature was chosen arbitrarily, the used approach does not guarantee that the pinch point temperature design parameter is adhered to in the evaporator. To check this the minimum pinch point temperature difference is determined. Because the slope of the heat source fluid temperature matches that of the working fluid in the evaporator, the pinch point can be calculated using the following equation

$$T_{pinch} = \frac{T_4 - T_3}{S_4 - S_3} \cdot (S_{evapin} - S_3) + T_{HTFout} - T_{evap} \tag{4.5}$$

If there is a mismatch between the prescribed pinch temperature and the computed value, the evaporator temperature in the next iteration is lowered or raised in accordance with this mismatch.

$$T'_{evap} = T_{evap} + (T'_{pinch} - T_{pinch}) \tag{4.6}$$

This process is repeated until a combination of operating points is found which complies to the pinch point temperature design parameter.

For the condenser the temperature slopes of the cooling and heating flows are also matched. However, because the condenser temperature is dictated by the minimal condensing pressure, no iterations are needed to compute temperature levels which comply with the design parameters. The inlet and output temperatures of the water flow are computed thusly

$$T_{waterout} = T_{cond} - T_{pinch} + (s_6 - s_7)\frac{T_6 - T_1}{s_6 - s_1} \tag{4.7}$$

$$T_{waterin} = T_{waterout} - (T_6 - T_1) \tag{4.8}$$

All operating points in the cycle have now been determined. Two examples of T-s plots resulting from different HTF input temperatures are shown in 4.2. For HTF input temperatures higher than shown in the right plot the shape of the T-s diagram doesn't change. The graph of the HTF

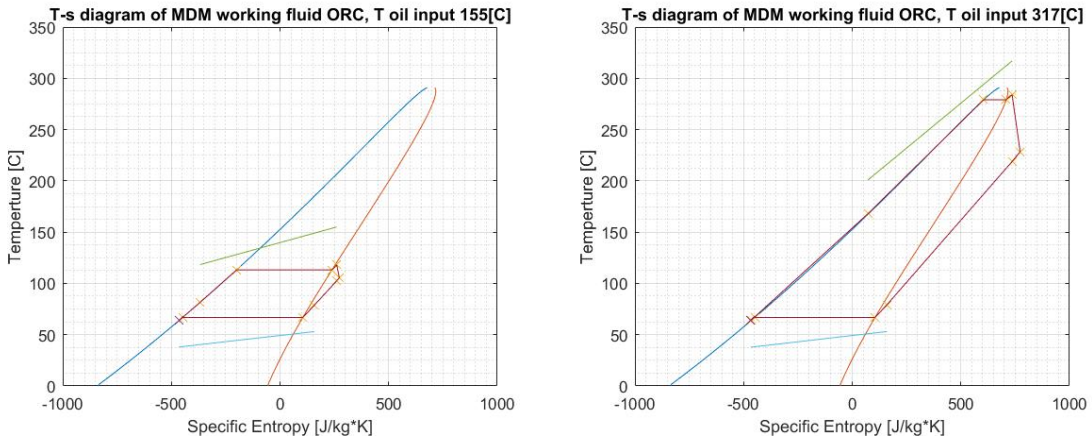

Figure 4.2: ORC plots for varying HTF input temperatures

temperature is shifted upward to indicate the higher heat source temperatures.

To ensure that energy is conserved using these operating points, the mass flows for the heat transfer fluid, working fluid and water are scaled.

Firstly, the mass flow of the working fluid is set so that the net work delivered by the cycle matches the rated electrical power. The specific net work of the cycle equals the specific work done by the turbine minus the specific work done by the pump. The expression for the mass flow of working fluid therefore is

$$\dot{m}_{wf} = \frac{P_e}{(h_4 - h_5) - (h_2 - h_1)} \tag{4.9}$$

The mass flows of the heat transfer fluid and the water are scaled by balancing the energy flows in the evaporator and the condenser.

$$\dot{m}_{HTF} = \frac{(h_4 - h_3)m_{wf}}{(T_4 - T_3)c_{HTFavg}} \tag{4.10}$$

$$\dot{m}_{water} = \frac{(h_6 - h_1)m_{wf}}{(T_6 - T_1)c_{wateravg}} \tag{4.11}$$

In which c_{HTFavg} and $c_{wateravg}$ refer to the average thermal capacity of the heat transfer fluid and water in the evaporator and condenser respectively. With all operating points and mass flows scaled the

4.1.3 ORC efficiency

The conversion efficiency of the ORC module determines, for a large part, the efficiency of the entire system. It is therefore one of the most important performance indicators of the system. The efficiency of the ORC is defined as such

$$\eta_{ORC} = \frac{W_{out} - W_{pump}}{Q_{in}} \tag{4.12}$$

With W_{out},W_{pump} and Q_{in} being the output power, pumping power and supplied heat respectively. Because a generator efficiency of 100 % is assumed the specific output power equals the enthalpy drop over the turbine. Similarly the specific supplied heat equals the enthalpy gain of the working fluid over the evaporator.

The pumping power is a combination of the pumping power required for the working fluid flow,w_{pwf}, and for the heat transfer fluid,w_{pHTF}. w_{pwf} is determined from the specific enthalpy increase in the pump.

The pumping power required for the HTF through the storage module is considered because it is significant with respect to the total power. The storage module consists of pipes which are tens of meters long. The large pressure gradient over these pipes results in considerable pumping power requirements. The length of these pipes is one of the variables of interest in the parameter study which will result in differing pumping powers. Furthermore, because the mass flow of the heat transfer fluid varies considerably for different input temperatures, the pumping power required for the HTF varies greatly within one discharge cycle. The formulas used to compute the pressure drop over the pipe is the Darcy-Weisbach equation whilst using the Haaland approximation for the friction factor.

$$\xi = -1.8 \log[(\frac{\epsilon/D_{tin}}{3.7})^{1.11} + \frac{6.9}{Re}] \tag{4.13}$$

$$f_D = (\frac{1}{\xi})^2 \tag{4.14}$$

$$\Delta P = f_D \frac{\rho_o \cdot u^2}{2 D_{tin} L} \tag{4.15}$$

With ϵ the roughness coefficient of the pipe material and u the bulk flow speed of the heat transfer fluid.

The pumping power for the HTF is computed from the pressure drop and the total mass flow of the HTF.

$$W_{pump,HTF} = \Delta P \cdot \dot{m}_{HTF} \tag{4.16}$$

For the verification process the HTF pumping power is not taken into account as the literature to which the model is compared doesn't do so either. However, in the result sections it is integrated in the total efficiency of the system.

4.1.4 ORC model verification

To verify the outcome of the ORC conversion model its results are compared to values reported in literature. The design parameters used comply with the paper of Fernandez [7]. The results of the model are compared to the results from that report to check if they comply. The parameter that is compared is the overall efficiency, this is done for several heat source outlet temperatures. This comparison is shown in 4.3. From this comparison it becomes clear that the overall calculated efficiency equals the values from literature. However, the efficiency drops of significantly faster with diminishing temperatures than the results found in literature. The overall shape of the two graphs are similar but the inflection point is not located at the same temperature.

These differences are explained by the fact that Fernandez uses other assumptions for its input temperature profiles. The report assumes that the input temperature of the HTF is constant, and instead adjusts only the HTF output temperature and flow speed. Therefore the same HTF output temperature does not guarantee the same evaporator temperature. This explains the shift in the inflection point and the difference in slope for lower temperatures.

When comparing the operational point data for the inflection points it is found that the temperature levels and energy flows comply. Therefore it is concluded that the model for the ORC is accurate.

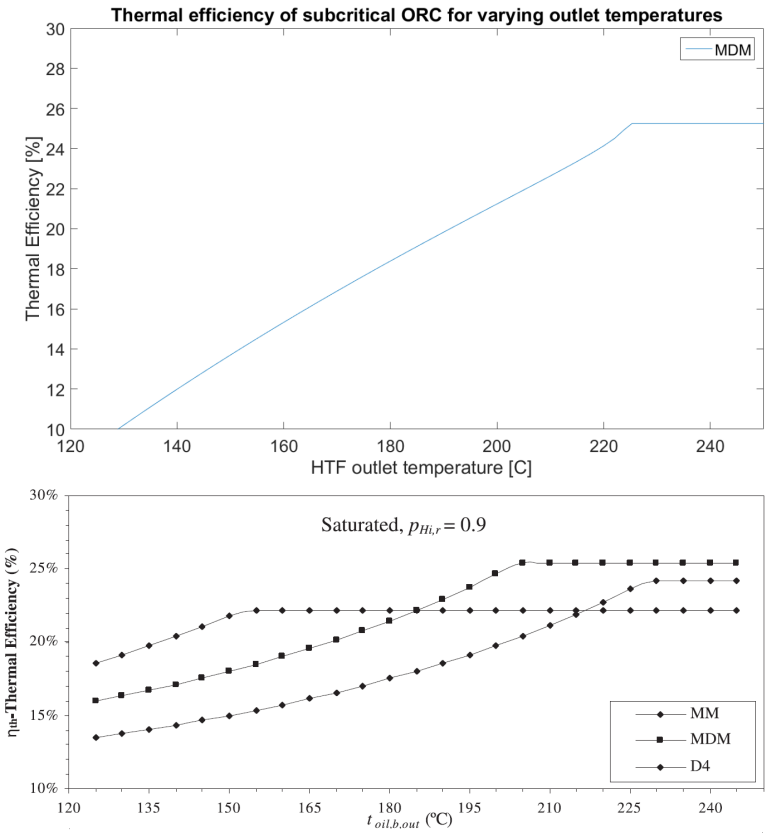

Figure 4.3: Comparison of simulated thermal efficiency with literature values

4.2 Storage Module

In the following section the mathematical model is used to model the behavior of the storage module is explained. As with the conversion module some assumptions in accordance with the relevant literature have been made to limit the design space. These assumptions will first be described after which the actual calculation method is explained.

4.2.1 Design parameters

Some of the design parameters of the storage module are set to be varied as part of the parameter study in the following chapter. Others, however, are fixed due to the fact that they are either specific to the Ecovat application or are dictated by material properties. All design parameters used in the base case are listed in the table below.

Variable	Range/Value	Motivation	Sources
E_e	$7.48 \cdot 10^3$ [kWh]	Required electricity storage capacity	Application
P_e	300 [kW]	Required electrical power	Application
T_{cmax}	643 [K]	Limited to critical temperature working fluid	Material
T_{cmin}	448 [K]	Cutoff to ensure minimal efficiency	ORC modeling
C_c	557 [K]	Cutoff to not exceed critical temperature	Material
L	20 [m]	Subject of parameter study	-
d_{pipe}	0.02 [m]	Subject of parameter study	-

Table 4.2: Boundary conditions for the storage module

4.2.2 Storage dimensions and segmentation

The overall storage size necessary is determined by the thermal storage capacity needed to achieve the goals of the system. The amount of thermal storage capacity is determined by the electric storage capacity and the average conversion efficiency. The thermal power needed is determined by the electric power and the minimal conversion efficiency. To limit the size of the storage module a minimum conversion efficiency of 10% and an average conversion efficiency of 12% are assumed.

$$E_{th} = \frac{E_e}{\eta_{avg}} \tag{4.17}$$

$$P_{th} = \frac{P_e}{\eta_{min}} \tag{4.18}$$

How much concrete is needed to store this amount of energy is calculated as follows

$$m_c = \frac{E_{th}}{c_c \cdot (T_{cmax} - T_{cmin})} \tag{4.19}$$

With c_c being the specific heat capacity of concrete, and T_{cmax} and T_{cmin} the maximum and minimum concrete temperature respectively. The maximum concrete temperature is determined by the maximum temperature allowed for the working fluid. The minimal concrete temperature is determined by the lowest temperature for which a conversion efficiency of at least 10% can be achieved.

Once the total amount of storage material which is needed is known, the number of heat exchanger pipes is determined. The preferred number of pipes is the minimum needed to ensure the needed thermal power can be supplied at the lowest output temperature. To extract the needed thermal power a certain HTF mass flow is needed. To determine the total HTF mass flow an HTF temperature increase of 33 degrees is assumed inside the storage module. This is lowest the temperature increase described by the ORC module over the entire relevant modeling range.

$$\dot{m}_{HTF} = \frac{P_{th}}{c_{HTF} \cdot T_{pinch}} \tag{4.20}$$

The number of pipes used in the concrete is minimized whilst allowing for the needed thermal power to be extracted. This is done by assuming an arbitrary starting number of pipes, n_{pipes}, calculating the overall heat transfer coefficient, determining the number of pipes needed with this heat transfer coefficient, and using the resulting value as the starting point for the next iteration.

Firstly the flow speed of the HTF inside the pipe is determined. After this step the heat transfer coefficient, h, is calculated. This step is elaborated upon in the internal heat transfer section

$$\dot{m}_{pipe} = \frac{\dot{m}_{HTF}}{n_{pipes}} \tag{4.21}$$

$$u_{HTF} = \frac{\dot{m}_{pipe}}{\rho_{HTF}} \cdot \frac{1}{A_{pipe}} \tag{4.22}$$

In which $\dot{m}_{pipe}$ is the mass flow through one of the pipes. u_{HTF} and ρ_{HTF} are the flowspeed of the HTF and A_{pipe} the flow area of the pipe.

The volume of the concrete around the pipe is determined by dividing the total needed volume of concrete by the number of pipes. The outer radius of the concrete is calculated at a given pipe length, L. The length of the pipes can be varied but must fit inside the tank, for the calculations a length of 20 meters was used.

$$V_c = \frac{m_c}{\rho_c} \tag{4.23}$$

$$V_{pipe} = \frac{V_c}{n_{pipes}} \tag{4.24}$$

$$R_c = \sqrt{\frac{V_c}{\pi \cdot N} + r_t^2} \tag{4.25}$$

With V_c the total volume of the concrete, V_{pipe} the concrete volume per pipe and r_c the radius of the concrete segment per pipe.

The heat transfer coefficient inside the pipe is used to arrive at an overall heat transfer coefficient from the concrete to the HTF. This overall heat transfer coefficient is used to determine the minimum number of pipes needed to achieve the needed thermal power, for an assumed pinch temperature of 10 degrees.

$$AU = L \cdot h \cdot \pi \cdot d_{pipe} \tag{4.26}$$

$$n_{pipes} = \frac{P_{th}}{AU \cdot T_{pinch}} \tag{4.27}$$

This new number of pipes is used as input for the next iteration of the calculation. Once the rounded value for the number of pipes needed to achieve the thermal power is stable, the iterative function is halted and the final value for the number of pipes is used in further calculations.

4.2.3 Internal heat transfer

The temperature and flow speed of the HTF varies continuously during the charge and discharge phases. Therefore, the heat transfer rate also varies and is reevaluated every time step, for each location. This is done by subsequent calculation of the flow speed, Reynolds number, Nusselt number and finally the heat transfer coefficient. The equations used for these calculations are listed below. Due to the pipes being very long in comparison to their diameter the flow is assumed to be fully developed and the fully developed regime is used for the entire pipe length.

The heat transfer coefficient is used to determine the thermal power flowing from the concrete into the HTF. The thermal power per unit length for each time interval and position along the pipe is calculated as follows

$$P_{th}(i,j) = h(i,j) \cdot D_{pipe} \cdot \pi \cdot \Delta z \cdot (T_{HTF}(i,j) - T_c(i,j,1)) \tag{4.28}$$

How he temperature of the concrete, T_c, used in this equation is determined, is discussed in the next section.

4.3 Concrete conduction model

To determine the charging and discharging behavior of the concrete storage module, the rectangular concrete block is subdivided into smaller cylindrical segments. Each cylindrical segment

corresponds to the concrete surrounding one of the heat exchanger pipes. The cylindrical geometry for the segments is used because of symmetry and modeling simplicity considerations. The radius of the cylinders is adjusted so that the total volume of the concrete is not altered. A schematic representation of how these cylinders are arranged within the rectangular concrete is shown in figure 4.4. The indicated diameters d_{tube} and d are equal to $2R_{tube}$ and $2R$ respectively.

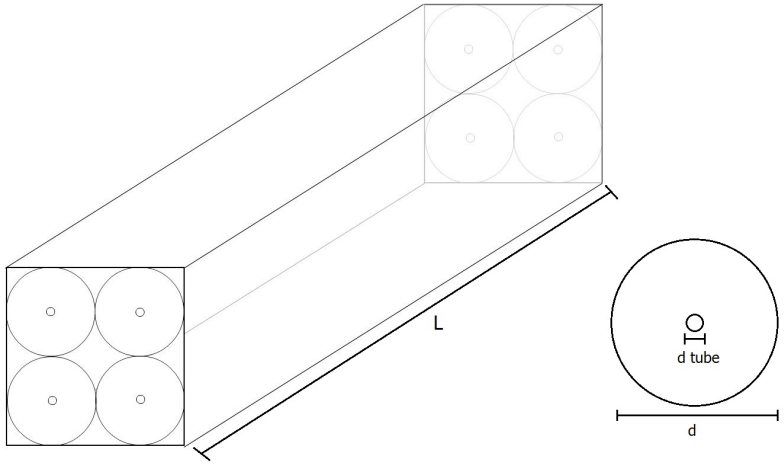

Figure 4.4: Schematic representation of some cylindrical segments inside the bulk concrete

A simplified version of the heat equation is used in conjunction with the finite difference method to develop a mathematical model for the temperature gradient inside the cylinders. To do this, firstly the governing equations and boundary conditions are determined and the discretization is discussed. Secondly the discretization is applied to the equations to arrive at a finite difference model of the storage module. The following section elaborates upon these steps and discusses how these are implemented.

4.3.1 Governing Equations and Boundary Conditions

To simplify the mathematical model a number of assumptions are made about the storage module and its behavior. These assumptions, along with the simplified version of the heat equation, are listed below.

1. The heat transfer through the segment is assumed to be rotationally symmetrical
2. The perimeter of the concrete section is perfectly insulated allowing heat to be added or extracted through the central tube only
3. The flow of the heat transfer fluid is fully developed and uniform in the entire pipe
4. The thermal resistance of the tube is negligible

$$\rho C \frac{\partial T}{\partial t} = -k\left(\frac{\partial^2 T}{\partial r^2} + \frac{1}{r}\frac{\partial T}{\partial r} + \frac{\partial^2 T}{\partial z^2}\right) \tag{4.29}$$

This equation holds for the domain $\Omega = (z, r) \in \mathbb{R} | 0 < z < L, R_{tube} < r < R$. On the boundary Γ of the domain Ω the following boundary conditions are applied.

$$\frac{\partial T}{\partial r}(z, R) = 0, 0 \leq z \leq L$$

$$\frac{\partial T}{\partial z}(0,r) = \frac{\partial T}{\partial z}(L,r) = 0, R_{tube} \leq r \leq R$$

$$-k\frac{\partial T}{\partial r}(z,R_{tube}) = h(T - T_\infty), 0 \leq z \leq L$$

In this equation T_∞ refers to temperature of the heat transfer fluid flowing through the pipe.

These boundary conditions correspond with an adiabatic outer layer of the cylinder, and convectional heat transfer between the concrete and the heat transfer fluid.

4.3.2 Discretization

A schematic representations of the modeled domain is shown in figure 4.5. During discretization the temperature at specific locations inside the concrete are used to determine temperature of the entire segment. These locations are referred to as nodes and are represented by the black dots in figure 4.5. The positions of the nodes and the inter nodal distances are defined as.

$$z_j = j\Delta z, j = 1(1)N, \Delta z = \frac{L}{N-1}$$

$$r_k = k\Delta r + R_{tube}, k = 1(1)M, \Delta r = \frac{(R - R_{tube})}{M-1}$$

$$t_i = i\Delta t, i = 1(1)O, \Delta t = \frac{t_{total}}{O-1}$$

The final expression defines the time discretization with a total simulated time t_{total} and a time step size of Δt.

The partial differential equation is integrated over time and applied to all the nodes, however the differential terms are replaced by their finite difference approximations. The finite difference approximations are defined using the central difference method and are listed below.

$$\frac{\partial T}{\partial t}|i,j,k = \frac{T^{i+1}_{j,k} - T^i_{j,k}}{\Delta t} \tag{4.30}$$

$$\frac{\partial^2 T}{\partial r^2}|_{j,k} = \frac{T_{j,k+1} - 2T_{j,k} + T_{j,k-1}}{\Delta r^2} \tag{4.31}$$

$$\frac{\partial T}{\partial r}|_{j,k} = \frac{T_{j,k+1} - T_{j,k-1}}{2\Delta r} \tag{4.32}$$

$$\frac{\partial^2 T}{\partial z^2}|_{j,k} = \frac{T_{j+1,k} - 2T_{j,k} + T_{j-1,k}}{\Delta z^2} \tag{4.33}$$

Furthermore, to enable multiple finite difference methods the variable θ is introduced. θ can assume the values of $1, 0$ and $\frac{1}{2}$ to utilize the Euler implicit, Euler explicit or Crank-Nicholson method respectively. The general discretized version of the differential equation with inclusion of the variable θ is

$$\tau^i = \frac{T^i_{j,k+1} - 2T^i_{j,k} + T^i_{j,k-1}}{\Delta r^2} + \frac{T^i_{j,k+1} - T^i_{j,k-1}}{2\Delta r} + \frac{T^i_{j+1,k} - 2T^i_{j,k} + T^i_{j-1,k}}{\Delta z^2} \tag{4.34}$$

$$\frac{T^{i+1}_{j,k} - T^i_{j,k}}{\Delta t} = (1-\theta)\cdot\tau^i + \theta\cdot\tau^{i+1} \tag{4.35}$$

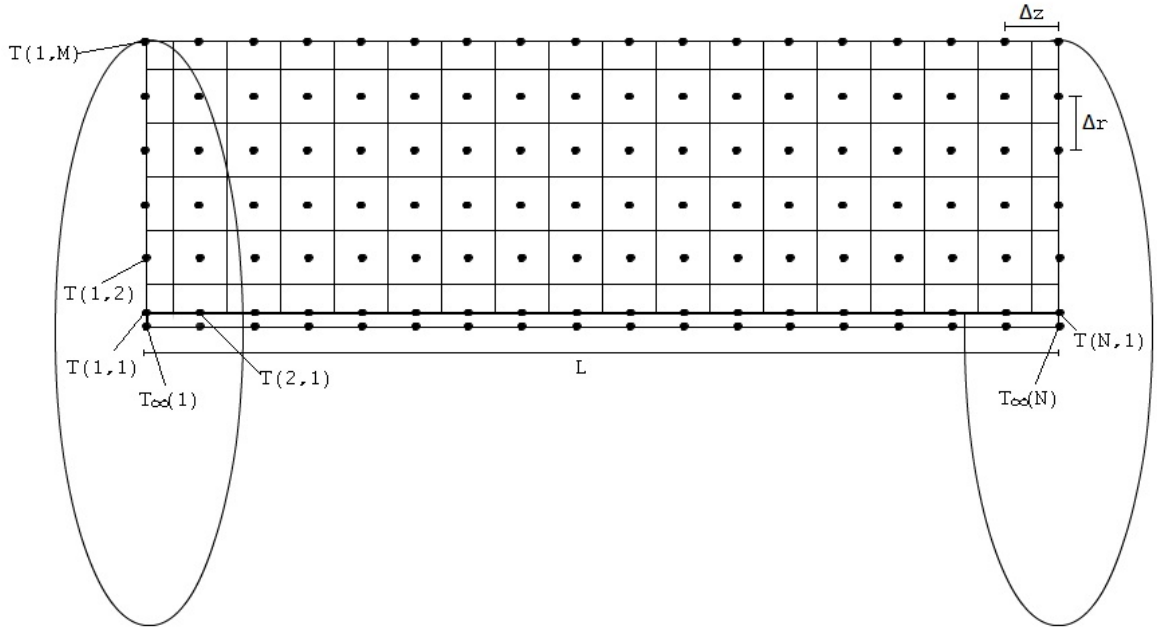

Figure 4.5: Schematic representation of concrete discretization

The fully discretized and integrated function using the Euler Implicit method is therefore as follows

$$T_{j,k}^{i} = T_{j,k}^{i+1} + \alpha\Delta t\left(\frac{T_{j,k+1}^{i+1} - 2T_{j,k}^{i+1} + T_{j,k-1}^{i+1}}{\Delta r^2} + \frac{1}{R_k}\frac{T_{j,k+1}^{i+1} - T_{j,k-1}^{i+1}}{2\Delta r} + \frac{T_{j+1,k}^{i+1} - 2T_{j,k}^{i+1} + T_{j-1,k}^{i+1}}{\Delta z^2}\right) \tag{4.36}$$

These approximations are abbreviated versions of the Taylor series expansions for first and second order derivatives. The omission of the higher order terms of the series results in a truncation error. However, because the size of the error scales with higher orders of Δr and Δz the error remains acceptable given sufficiently small values for Δr and Δz.

When these discretization methods are applied to the boundary Γ some adjustments needs to be made. To illustrate this consider the nodes $T_{j,M}$. To perform the central difference method approximation the nodes $T_{j,M-1}$ and $T_{j,M+1}$ need to be known , but the nodes $T_{j,M+1}$ are not defined and are considered 'ghost nodes'.

However, the boundary condition $\dfrac{\partial T}{\partial r}(R, z) = 0, 0 \leq z \leq L$ states after discretization that

$$\frac{T_{j,M+1} - T_{j,M-1}}{2\Delta r} = 0 \tag{4.37}$$

This implies that $T_{j,M+1} = T_{j,M-1}$ which is used in the approximations of the second order terms of the PDE. The same procedure can be used for the other adiabatic sections of Γ.

In the section of Γ where the boundary condition is convective the ghost node approach is also

applied. The boundary condition in this region is

$$k\frac{\partial T}{\partial r}(R_{tube}, z) = h(T - T_\infty), 0 \leq z \leq L \tag{4.38}$$

After discretization the following expression is found for the nodes in the region $T_{j,1}$.

$$k\frac{T_{j,2} - T_{j,0}}{2\Delta r} = h(T_{j,1} - T_\infty) \tag{4.39}$$

after rearranging the following expression is found for the ghost nodes $T_{k,0}$.

$$T_{j,0} = T_{j,2} - \frac{2h\Delta r}{k}(T_{j,1} - T_\infty) \tag{4.40}$$

These boundary conditions result in the following Euler implicit function for the nodes adjacent to the heat exchanger pipe.

$$T^i_{j,1} = T^{i+1}_{j,1} + \alpha\Delta t\left(\frac{2T^{i+1}_{j,2} - 2T^{i+1}_{j,1} - \frac{2h\Delta r}{k}(T^{i+1}_{j,1} - T^{i+1}_\infty)}{\Delta r^2} + \frac{1}{R_1}\frac{h}{k}(T^{i+1}_{j,1} - T^{i+1}_\infty) + \frac{T^{i+1}_{j+1,1} - 2T^{i+1}_{j,1} + T^{i+1}_{j-1,1}}{\Delta z^2}\right) \tag{4.41}$$

Because the Euler implicit and Crank-Nicholson discretization schemes are used the system of equations and boundary conditions is solved using the linear solver of Matlab. How the equations are implemented in Matlab to achieve this is discussed in the next section.

4.3.3 Solving the system of equations

The linear solve function of Matlab can be used to solve systems of linear equations. The way it operates is that when given the equation, $\mathbf{Ab} = \mathbf{c} + \mathbf{d}$ and matrix and vector $\mathbf{A}$ and $\mathbf{c}$ are known, the function will return the vector $\mathbf{b}$.

For the purposes of this report the matrix and vectors need to be constructed in such a way that they allow for a two dimensional problem, which can be solved both explicitly as implicitly. Firstly, the vector $\mathbf{b}$ is arranged for a two dimensional problem. The nodes are arranged by row, after all the nodes of the first row the first node of the second row starts until the entire grid is entered.

$$\mathbf{b} = (T^{i+1}_{1,1}, \cdots, T^{i+1}_{1,M}, \cdots, T^{i+1}_{N,1}, \cdots, T^{i+1}_{N,M})^T \tag{4.42}$$

The matrix $\mathbf{A}$ is a $M \cdot N \times M \cdot N$ matrix which contains the coefficients of the partial differential equation for which the vector $\mathbf{b}$ is either the input and/or output (depending on the chosen method). The matrix is structured as a tridiagonal matrix with additional non zero diagonals on the $(M + 1)$ and the $-(M + 1)$ diagonal to incorporate the coefficients for the axial dimension. The boundary conditions cause the first and last terms of the three main diagonals to differ from the rest, as well as the first M or last M terms of the $(M+1)$ and $-(M+1)$ diagonals respectively. A short overview of how the matrix is constructed is given below, as well as an overview of the vector $\mathbf{c}$. For brevity some of the coefficients are combined into constants.

$$\beta = 2\frac{\alpha\Delta t}{(\Delta r)^2} \tag{4.43}$$

$$\gamma = \beta(1 + \frac{h}{k}\Delta r - \frac{\alpha\Delta t h}{kR} + 2\frac{(\Delta r)^2}{(\Delta z)^2}) \tag{4.44}$$

$$\zeta = \beta \frac{(\Delta r)^2 + (\Delta z)^2}{(\Delta z)^2} \tag{4.45}$$

$$\mu = \frac{\alpha \Delta t}{r(k,j) 2 \Delta r} \tag{4.46}$$

$$\mathcal{A} = \begin{bmatrix} 1+\theta\gamma & -\theta\beta & & & & \\ -\theta\beta+\mu & 1+\theta\zeta & -\theta\beta-\mu & & & \\ & \cdot & \cdot & \cdot & & \\ & & \cdot & \cdot & \cdot & \\ & & & -\theta\beta+\mu & 1+\theta\zeta & -\theta\beta-\mu \\ & & & & -2\theta\beta & 1+\theta\zeta \end{bmatrix} \tag{4.47}$$

$$\mathcal{D} = \begin{bmatrix} -\theta\frac{\alpha\Delta t}{(\Delta z)^2} & & & & & \\ & -\theta\frac{\alpha\Delta t}{(\Delta z)^2} & & & & \\ & & \cdot & & & \\ & & & \cdot & & \\ & & & & -\theta\frac{\alpha\Delta t}{(\Delta z)^2} & \\ & & & & & -\theta\frac{\alpha\Delta t}{(\Delta z)^2} \end{bmatrix} \tag{4.48}$$

$$\mathbf{A} = \begin{bmatrix} \mathcal{A} & 2\mathcal{D} & & \\ \mathcal{D} & \mathcal{A} & \mathcal{D} & \\ & \cdot & \cdot & \cdot \\ & \mathcal{D} & \mathcal{A} & \mathcal{D} \\ & & 2\mathcal{D} & \mathcal{A} \end{bmatrix} \tag{4.49}$$

$$\mathbf{d} = To_j^i[\beta(\frac{h}{k}\Delta r - \frac{\alpha \Delta t h}{kR}), 0, \cdots, 0] \tag{4.50}$$

$$\mathbf{c} = \tag{4.51}$$

$$\left[\begin{array}{c}
(1-(1-\theta)\gamma)T^i_{1,1} + 2(1-\theta)\beta T^i_{1,2} + 2(1-\theta)\frac{\alpha\Delta t}{(\Delta z)^2}T^i_{2,1} + T^i_{HTF,1}[\beta(\frac{h}{k}\Delta r - \frac{\alpha\Delta th}{kR})] \\
((1-\theta)\beta-\mu)T^i_{1,1} + (1-(1-\theta)\zeta)T^i_{1,2} + ((1-\theta)\beta+\mu)T^i_{1,3} + 2(1-\theta)\frac{\alpha\Delta t}{(\Delta z)^2}T^i_{2,2} \\
\vdots \\
((1-\theta)\beta-\mu)T^i_{1,M-2} + (1-(1-\theta)\zeta)T^i_{1,M-1} + ((1-\theta)\beta+\mu)T^i_{1,M} + 2(1-\theta)\frac{\alpha\Delta t}{(\Delta z)^2}T^i_{2,M-1} \\
2(1-\theta)\beta T^i_{1,M-1} + (1-(1-\theta)\zeta)T^i_{1,M} + 2(1-\theta)\frac{\alpha\Delta t}{(\Delta z)^2}T^i_{2,M}
\end{array}\right]$$

$$\left[\begin{array}{c}
(1-\theta)\frac{\alpha\Delta t}{(\Delta z)^2}T^i_{1,1} + (1-(1-\theta)\gamma)T^i_{2,1} + 2(1-\theta)\beta T^i_{2,2} + (1-\theta)\frac{\alpha\Delta t}{(\Delta z)^2}T^i_{3,1} + T^i_{HTF,2}[\beta(\frac{h}{k}\Delta r - \frac{\alpha\Delta th}{kR})] \\
(1-\theta)\frac{\alpha\Delta t}{(\Delta z)^2}T^i_{1,2} + ((1-\theta)\beta-\mu)T^i_{2,1} + (1-(1-\theta)\zeta)T^i_{2,2} + ((1-\theta)\beta+\mu)T^i_{2,3} + (1-\theta)\frac{\alpha\Delta t}{(\Delta z)^2}T^i_{3,2} \\
\vdots \\
(1-\theta)\frac{\alpha\Delta t}{(\Delta z)^2}T^i_{1,M-1} + ((1-\theta)\beta-\mu)T^i_{2,M-2} + (1-(1-\theta)\zeta)T^i_{2,M-1} + ((1-\theta)\beta+\mu)T^i_{2,M} + (1-\theta)\frac{\alpha\Delta t}{(\Delta z)^2}T^i_{3,M-1} \\
(1-\theta)\frac{\alpha\Delta t}{(\Delta z)^2}T^i_{1,M} + 2(1-\theta)\beta T^i_{2,M-1} + (1-(1-\theta)\zeta)T^i_{2,M} + (1-\theta)\frac{\alpha\Delta t}{(\Delta z)^2}T^i_{3,M}
\end{array}\right]$$

$$\left[\begin{array}{c}
2(1-\theta)\frac{\alpha\Delta t}{(\Delta z)^2}T^i_{N-1,1} + (1-(1-\theta)\gamma)T^i_{N,1} + 2(1-\theta)\beta T^i_{N,2} + T^i_{HTF,N}[\beta(\frac{h}{k}\Delta r - \frac{\alpha\Delta th}{kR})] \\
2(1-\theta)\frac{\alpha\Delta t}{(\Delta z)^2}T^i_{N-1,2} + ((1-\theta)\beta-\mu)T^i_{N,1} + (1-(1-\theta)\zeta)T^i_{N,2} + ((1-\theta)\beta+\mu)T^i_{N,3} \\
\vdots \\
2(1-\theta)\frac{\alpha\Delta t}{(\Delta z)^2}T^i_{N-1,M-1} + ((1-\theta)\beta-\mu)T^i_{N,M-2} + (1-(1-\theta)\zeta)T^i_{N,M-1} + ((1-\theta)\beta+\mu)T^i_{N,M} \\
2(1-\theta)\frac{\alpha\Delta t}{(\Delta z)^2}T^i_{N-1,M-1} + 2((1-\theta)\beta-\mu)T^i_{N,M-1} + (1-(1-\theta)\zeta)T^i_{N,M}
\end{array}\right]$$

The order of the nodes in vector **c** is the same as that used in **b**. However, to solve (semi) explicit systems the expression representing those nodes needs to contain the discretized form of the PDE including the boundary conditions. The resulting vector **c** has terms, when expressed in symbolic form are quite long and cluttered. This is due to the two dimensional approach, combined with the fact that implicit as well as explicit solution schemes need to be accommodated.

4.3.4 Verification

To verify the finite difference method described in the previous section, it is compared with analytical solutions. The main objective of this step is to determine what the minimum amount of nodes in each direction is that is needed to achieve accurate results.

The first analytical solution which is used is that of a semi infinite solid which is subjected to a convective heat transfer at its boundary. This first step in the verification procedure is meant to verify the results in the radial direction only. Therefore variations in the axial direction are not taken into account. The analytical solution for the temperature distribution in such a solid is.

$$\frac{Tc_{x,t} - T_i}{T_\infty - T_i} = erfc(\frac{x}{2\sqrt{\alpha t}}) - exp(\frac{hx}{k} + \frac{h^2\alpha t}{k^2})erfc(\frac{x}{2\sqrt{\alpha t}} + \frac{h\sqrt{\alpha t}}{k}) \tag{4.52}$$

This solution only holds for a semi infinite solid in Cartesian coordinates. Therefore, the radial finite difference solution needs to be altered to resemble its form in a Cartesian coordinate system, before the solutions can be accurately compared. This is done by drastically increasing the inner tube diameter R_{tube}. By doing this the radius of the concrete becomes negligible in comparison

to the inner diameter. This results in a small relative difference between the inner and outer circumference of the concrete, which approximates a flat plate.

Another difference between the studied problem and the semi-infinite solid solution is the boundary condition. The analytical solution assumes an infinitely extending solid. However the finite difference derivation assumes an insulated boundary. To overcome this discrepancy the section that is compared to the analytical solution is only one fifth of the total radius that is modeled. By using this approach the studied segment is not affected by the boundary condition if the simulated time is sufficiently short. The number of nodes is scaled with the total radius that is modeled. In that way the amount of nodes used for the studied section is not affected by the increased radius of the modeled section.

The first step is to determine how many radial nodes are needed for the discretized approach. To do this a one hour charging scenario is modeled using the Crank-Nicholson scheme and compared to the analytical solution. With a concrete starting temperature of 373 K and a uniform heat transfer fluid temperature of 563 K. The radius of the concrete segment is set at 0.2 meters and the outer diameter of the heat exchanging pipe is 100 m. The heat transfer coefficient, specific heat, density and mass flow of the heat transfer fluid are all kept constant during the simulation. In the axial direction only two nodes are used resulting in one large segment in the axial direction. The results are compared to the analytical solution. The results for this comparison are shown in figure 4.6.

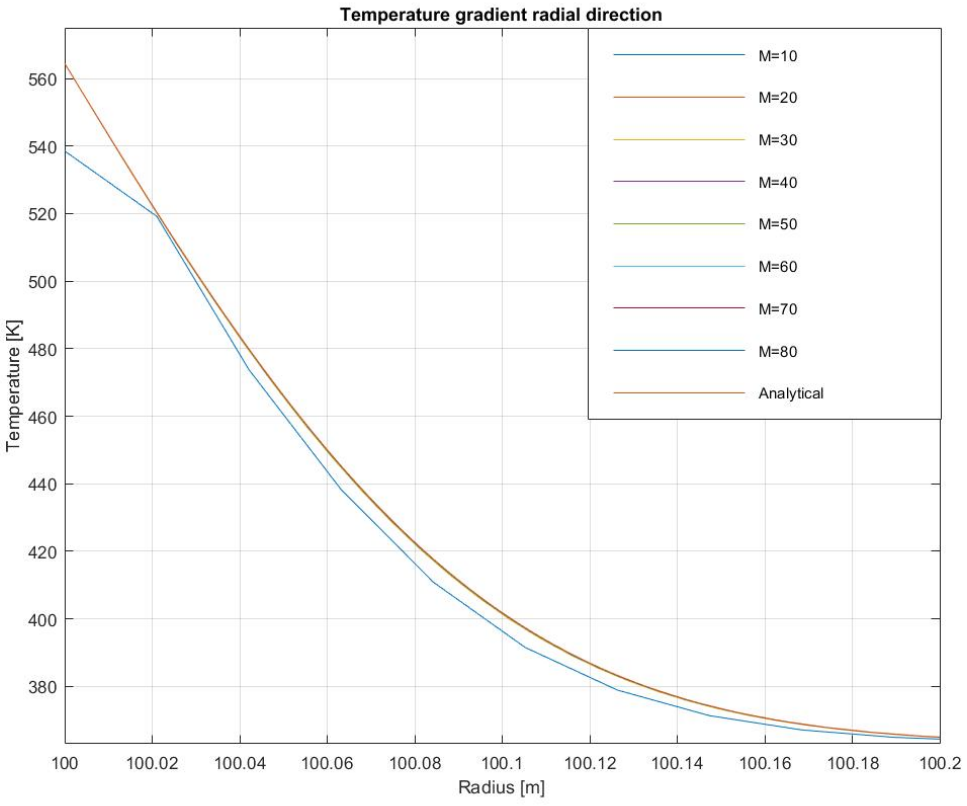

Figure 4.6: Temperature gradient for varying amounts of radius nodes

As can be seen from the figures the finite difference calculation method complies well with the

analytical solution for all but the fewest amount of radial nodes. The system of equations was solved using the the Crank-Nicholson scheme. The inaccurate results of the 10 node solution could be improved by using the Euler implicit scheme for the first radial node. However due to the overall poor accuracy of this solution improving this solution was not pursued. To maintain accurate results the timestep size dt equals the characteristic diffusion time $t_{dif} = \frac{dr^2}{\alpha}$, with α being the thermal diffusivity of the concrete. Because t_{dif} is dependent on the number of radial nodes the time steps varies for different node numbers. Good compliance with the analytical solution is observed from 20 radial nodes onward. However, to obtain a more precise gage of the accuracy of the different solutions, a second test is performed.

The second test compares the energy increase of the concrete with the energy supplied to the concrete by the heat transfer fluid. The energy absorbed by the concrete and the energy supplied to the concrete are computed using the following formulas.

$$E_{tot} = \sum_{j=1}^{M} \sum_{k=1}^{N} C_{j,k}(T_{j,k}^{Time} - T_{j,k}^{1}) \tag{4.53}$$

$$E_{in} = \sum_{t=1}^{Time} hA(T_{1,1}^{i} - T_{HTF})\Delta t \tag{4.54}$$

$$\epsilon = \frac{E_{tot}}{E_{in}} \tag{4.55}$$

With $C_{j,k}$ the thermal capacity of the segment and A the heat exchanging surface. For this test no segmentation is applied in the axial direction and the heat transfer fluid temperature To is assumed to be constant. ϵ indicates the degree to which the two solutions comply with a value of 1 indicating total compliance. The results of this test are shown in table 4.3. These results indicate

M	ϵ
20	0.821
30	0.930
40	0.963
50	0.977
60	0.984
70	0.989
80	0.991
90	0.993
100	0.994

Table 4.3: Compliance between analytical and numerical solution for different radial node amounts

that the error between the two estimated values is less than 1% when 80 or more nodes are used in the radial direction. Therefore this number of nodes is chosen as this amount of precision is sufficient for the intended purpose. 4.7 shows the temperature evolution over time in the concrete segment during constant temperature charging.

The previous results have all assumed no axial segmentation and therefore a constant heat transfer fluid temperature. To model the temperature change of the heat transfer fluid along the pipe length the following formula is used.

$$T_{HTF,j+1}^{i} = T_{HTF,j}^{i} + \frac{h_j^i A(T_{j-1,1}^{i} - T_{HTF,j-1}^{i})}{\dot{m}_{HTF} C_{HTF}} \tag{4.56}$$

$T_{HTF,j}^{i}$ refers to the temperature of the heat transfer fluid at position j along the Z axis, $\dot{m}$ refers to the mass flow of the HTF along through the pipe.

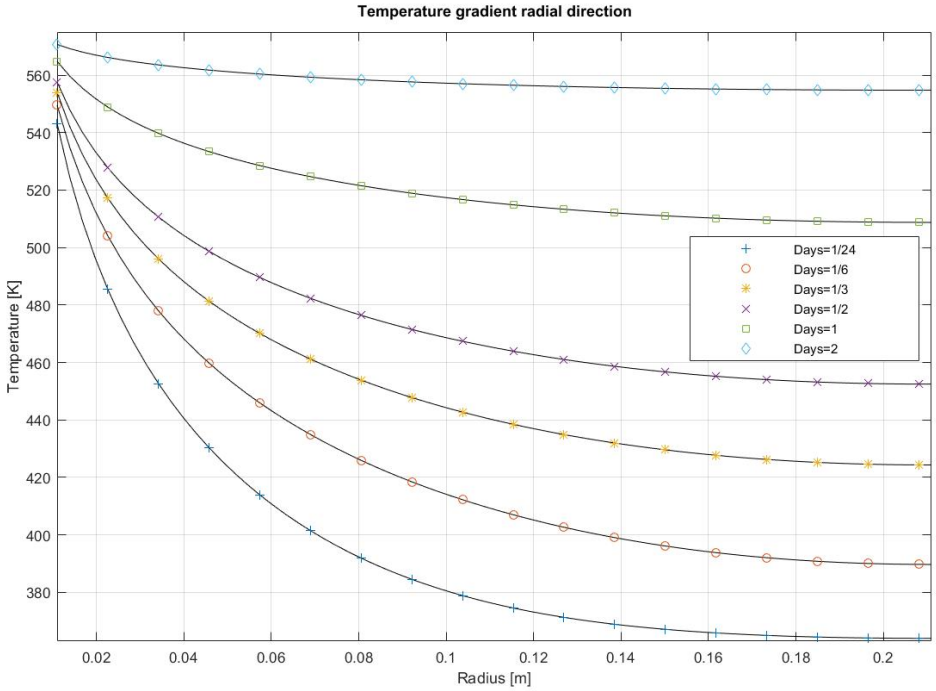

Figure 4.7: Time evolution of temperature gradient

N	ϵ
5	0.922
10	0.955
15	0.964
20	0.969
25	0.971

Table 4.4: Compliance to analytical solution of two dimensional simulation for varying axial node amounts

To determine how many axial nodes are needed to arrive at an accurate result, the same energy balance technique is used as for the radial nodes. However, because the heat transfer fluid temperature is not assumed to be constant anymore, the expression for E_{in} needs to be altered. The new expression uses the temperature difference between the fluid entering and exiting the heat transfer pipe,to determine the energy which is lost from the heat transfer fluid per time step.

$$E_{in} = \sum_{t=1}^{Time} \dot{m} C_{HTF} (To_1^i - To_{N\cdot(M-1)+1}^i) \Delta t \tag{4.57}$$

A similar analysis is performed where the total added heat content of the concrete is compared to the heat extracted from the heat transfer fluid. This comparison is performed whilst using 80 radial nodes. The results are shown in table 4.4. The number of axial nodes has a large influence on the total computational time needed to complete the simulation. Therefore a modest number of 15 axial nodes is chosen for the simulation. 15 nodes allows for a reasonable simulation time whilst providing reasonable accuracy.

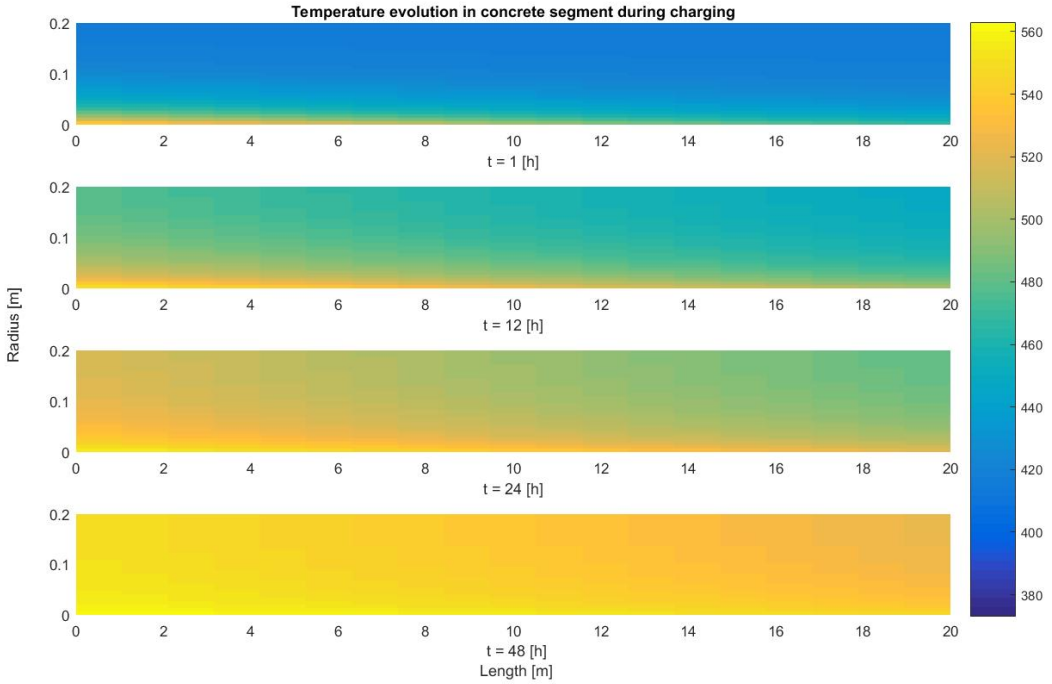

Figure 4.8: Temperature distribution in concrete segment during charging

With both radial and axial dependency incorporated 2-dimensional simulations are possible. Graphic representations of the temperature distribution inside a concrete segment after several charging times is shown in figure. These results correspond to 1, 12, 24 and 48 hours of charging with an input temperature of 573 K and a starting temperature of 363 K.

To arrive at a complete model of the system the output of the storage module is used as the input for the ORC module, and vice versa. The results of the charging and discharging behavior of this system are shown in the next chapter.

Chapter 5

Simulation Results

The model described in the previous chapter is used to model several charge and discharge scenario's. These scenario's are relevant for the application of the storage and conversion modules. Firstly the model for the ORC module is used to determine the appropriate operating range for efficient energy conversion. Secondly the base case system configuration mentioned in previous chapters is tested in two distinct scenario's: constant power and user profile. The parameters of the base case are then altered to assess the impact of the parameters on the results for the different scenario's.

5.1 Operating range of the conversion module

The temperature range at which the ORC module can operate directly influences the size of the storage module. Therefore it is desirable to have a large temperature range. However, the lower and upper bounds of the temperature range are dictated by efficiency and material restrictions. The temperature range influences a number of aspects of the ORC, two of which will be discussed below. These are:

- Efficiency

- Turbine size

These parameters can have detrimental effects on the system costs and/or storage module performance when they exceed their respective operating ranges.

5.1.1 Efficiency

The efficiency of the conversion module is one of the main performance indicators of the system. Furthermore, a minimum value of 10 % is demanded during the full discharge cycle. The conversion efficiency of an ORC is predominantly determined by the inlet temperature of the HTF. Therefore the inlet temperature has a lower limit which is allowed to ensure the minimum value. The efficiency of the ORC module is modeled for a range of inlet temperatures, the results of which are shown in figure5.1. As can be seen from the figure the minimal conversion efficiency of 10% cannot be guaranteed for inlet temperatures lower than 440 degrees centigrade. Therefore this temperature is set as the temperature at which the storage module is considered fully discharged.

The upper temperature bound for the storage module is dictated by the material which is used for the HTF. The HTF used in the model is Therminol 66 which has a critical temperature of 653 degrees Kelvin. To make sure the critical temperature of the HTF is not reached within the storage module the upper limit for the storage temperature is set at 650 degrees K. This upper

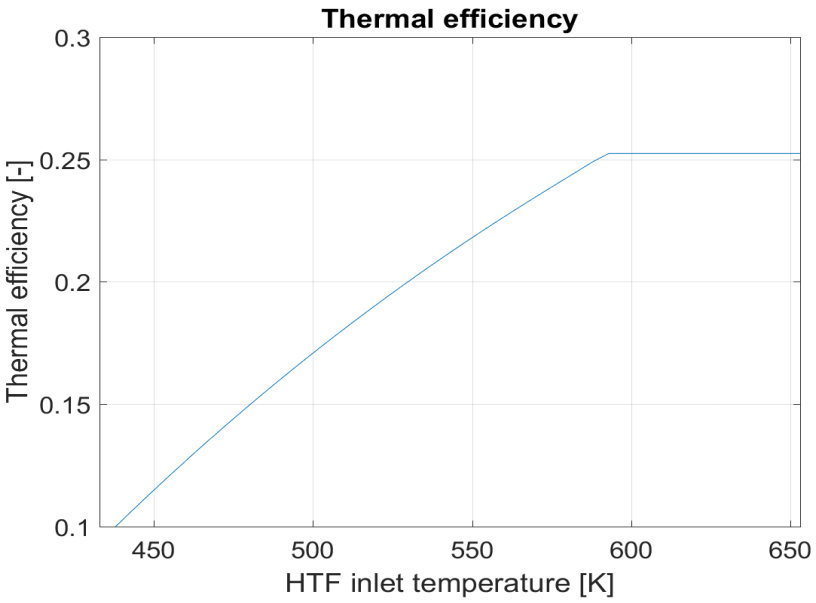

Figure 5.1: Thermal efficiency of sub-critical ORC for varying inlet temperatures

limit is within, but close to the maximum of, the allowable range for reinforced concrete.

5.1.2 Turbine Size

The component size of the different parts within the ORC module is not part of the scope of this report. However, the size of the turbine can influence the operating range of the entire system. This is because for certain working fluid and operating temperature combinations, the turbine would have to be unfeasibly large to supply the needed power. In the report of Maraver an approximation is put forth to estimate the size of a turbine, along with an acceptable range of between 0.02 and 1 m. The size parameter of the turbine needed for the ORC used in this report is 0.16 m and is therefore of no influence on the operating range.

5.2 Combined system

In this section the results of the charge and discharge simulations of the combined system are reported. Firstly, the charging and discharging behavior of the base case are considered. Secondly, the impact of the parameter alterations on the discharging behavior are studied. In figure 5.2 a schematic representation of the system is shown.

5.2.1 Initial setup

The initial setup refers to the setup discussed in the previous chapters. The parameters used in this scenario are summarized in the table below. During discharge simulations a usage profile taken from NEDU is used. NEDU is an organization which maps the electricity usage of Dutch households. The profile describes the energy usage during 2 consecutive winter days. The used electric power is scaled so that the total consumed energy matches the energy usage of 300 Dutch households in winter. A plot of the consumption curve is shown in figure 5.3. The results of the full discharge simulation of the initial setup are shown in figures 5.4 and 5.5.

During discharge the conversion efficiency remained well above the dictated minimum of 10%.

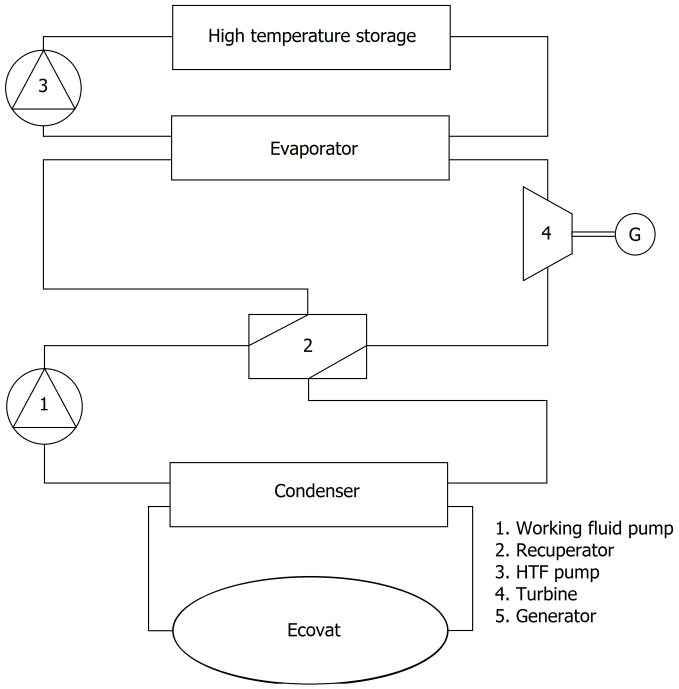

Figure 5.2: Schematic representation of ORC connected to the storage module

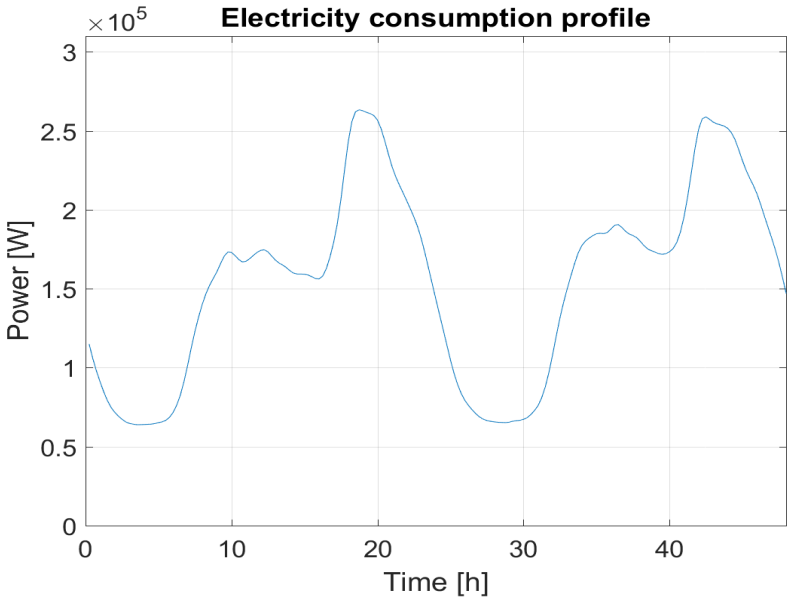

Figure 5.3: Consumption profile used in discharge simulations, created from data from [16]

However, the setup was not able to supply the required power for the full duration of the simulation, as the efficiency dropped drastically after the 42 hour mark. The simulation was aborted once the efficiency dropped below the minimum value of 10%. The efficiency dropped due to a cold region which had developed along the full length of the heat exchanger pipe. The temperature development inside the storage module is visualized in figure 5.6. Note the cold region at the bottom right region of the final subplot, which corresponds to the exit of the heat exchanger pipe. Because the simulation was halted prematurely, the storage module still contains 17.62% of its

Parameter	Value	Unit
Electric capacity	7.48	[MWh]
Thermal capacity	35.6	[MWh]
Electrical power	300	[kW]
Thermal power	3000	[kW]
Total storage volume	374	[m3]
Length	20	[m]
Segment Radius	0.1050	[m]
Pipe diameter	0.022	[m]
Number of Pipes	545	[-]
Average efficiency	0.21	[-]
Minimal efficiency	0.1	[-]

Table 5.1: Parameters of the initial setup configuration

initial charge at the time it is aborted.

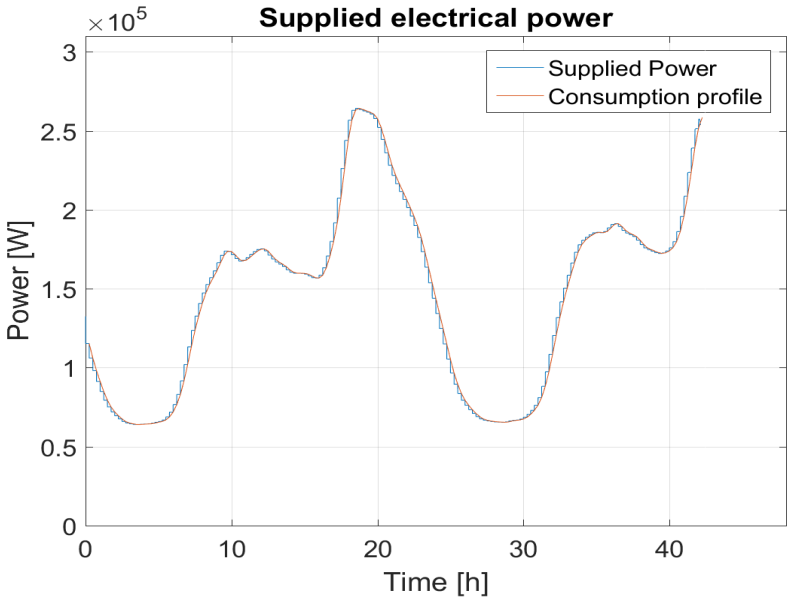

Figure 5.4: Supplied power and consumption profile during discharge simulation of starting setup

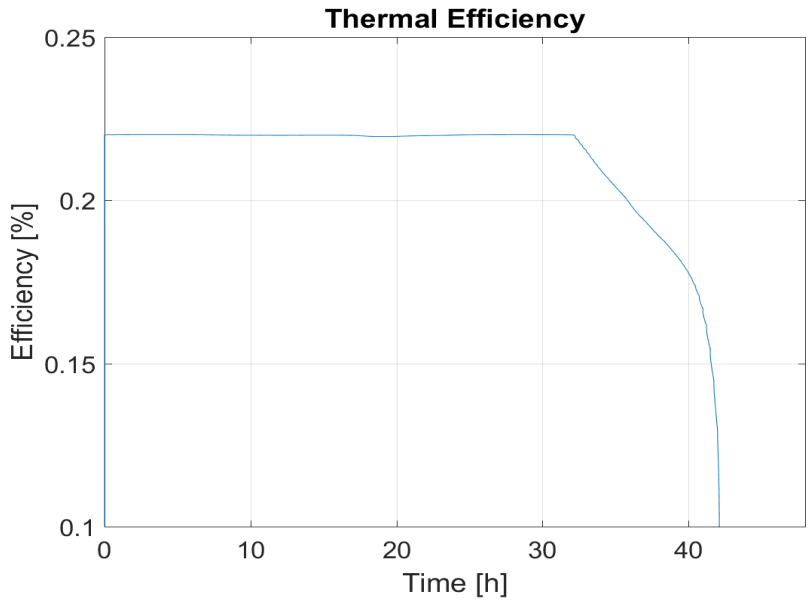

Figure 5.5: Thermal conversion efficiency of the ORC during discharge simulation

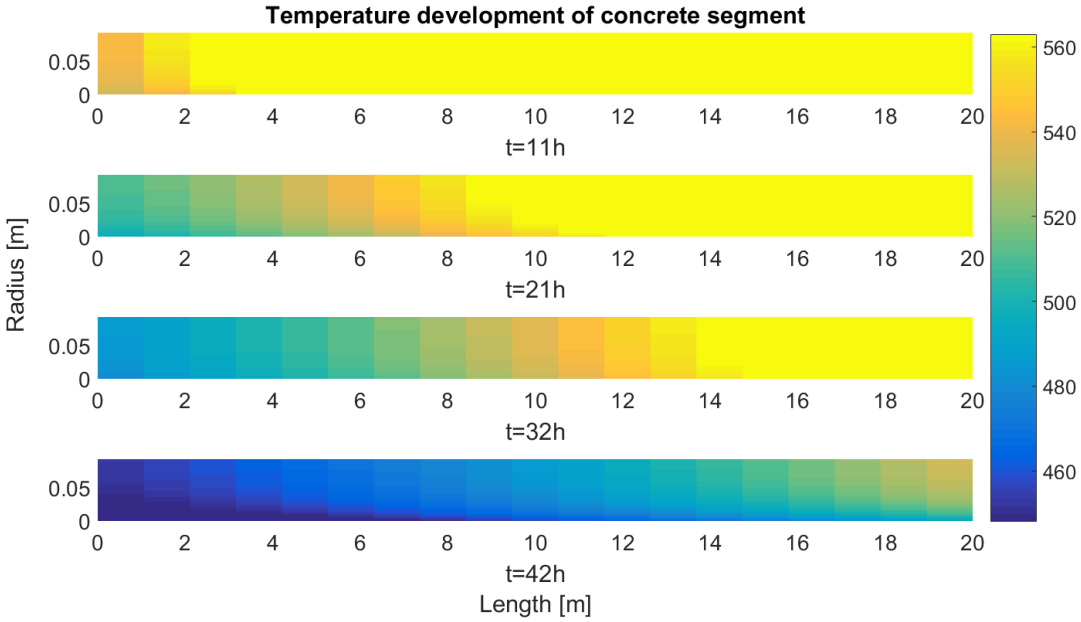

Figure 5.6: Concrete segment temperature development during discharge

5.2.2 Base Case

Without altering the performance conditions of the system several options are possible to improve the performance of the system. Two of these options are increasing either storage size or heat exchanger surface area. Due to cost considerations it was opted to increase the storage size of the system, as the storage material is cheaper than investing in more heat exchanging surface. The total volume of concrete was increased by 20%, this configuration will for the rest of this chapter be referred to as the base case. The parameters which have been updated are listed in the table below.

Parameter	Value	Unit
Electric capacity	8.98	[MWh]
Thermal capacity	42.72	[MWh]
Total storage volume	448	[m3]
Segment diameter	0.115	[m]

Table 5.2: Parameter adjustments made to initial setup to arrive at the base case

The discharge experiment was repeated for the base case. The results of this simulation are shown in figures 5.7 and 5.8. The increased concrete volume allows the system to adhere to the desired supply curve for the full duration of the simulation. The average efficiency during the discharge period is 21.15% and after 48 hours of discharge 16.4% of the initial charge remains. After the window of 48 hours the system was still able to keep discharging for an additional 9.5 hours. At the end of the full 57.5 hours of discharge the SOC was 3.62%.

The results of the full power discharge simulation of the base case are shown in figures 5.9 and 5.10. Due to the higher power the concrete region near the heat exchanger tube discharges quickly. This results in a quickly dropping HTF temperature and conversion efficiency. The average efficiency during the discharge is but already dalls below the critical value of 10% after 17.55 hours. After this time 22.82 % of the original charge still remained in the storage module.

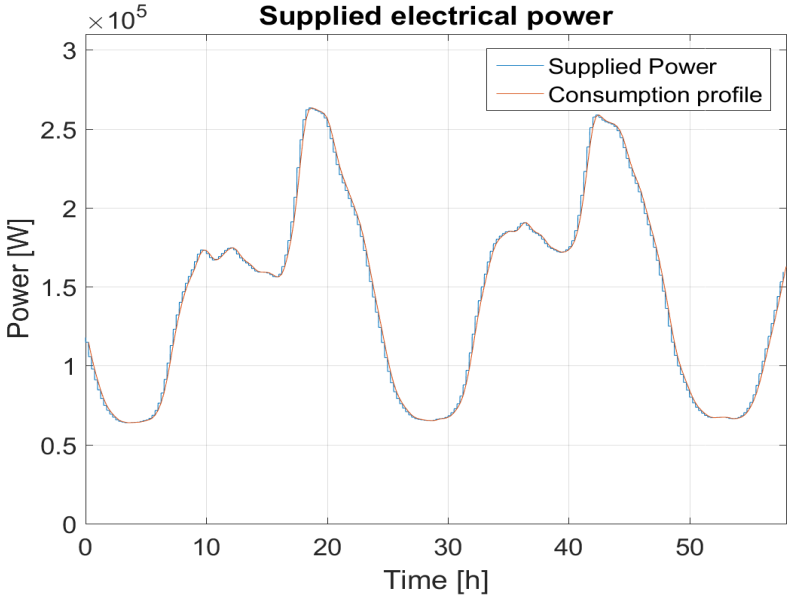

Figure 5.7: Supplied power and consumption profile during discharge simulation of base case

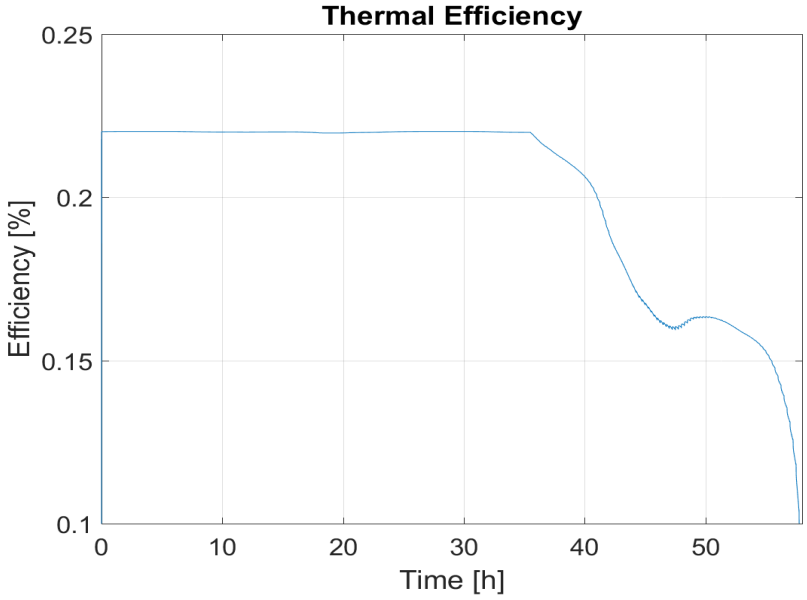

Figure 5.8: Thermal conversion efficiency of the ORC during discharge simulation of base case

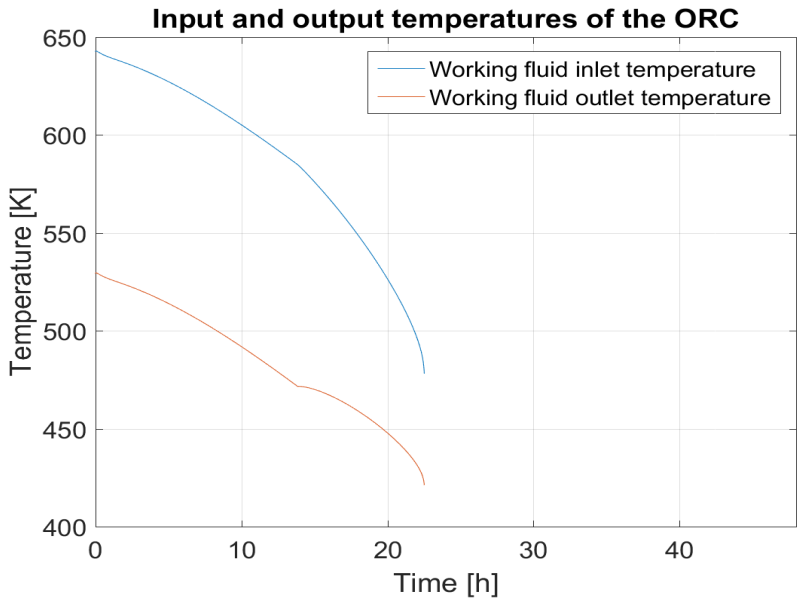

Figure 5.9: Inlet and outlet temperature of the ORC for during full power discharge

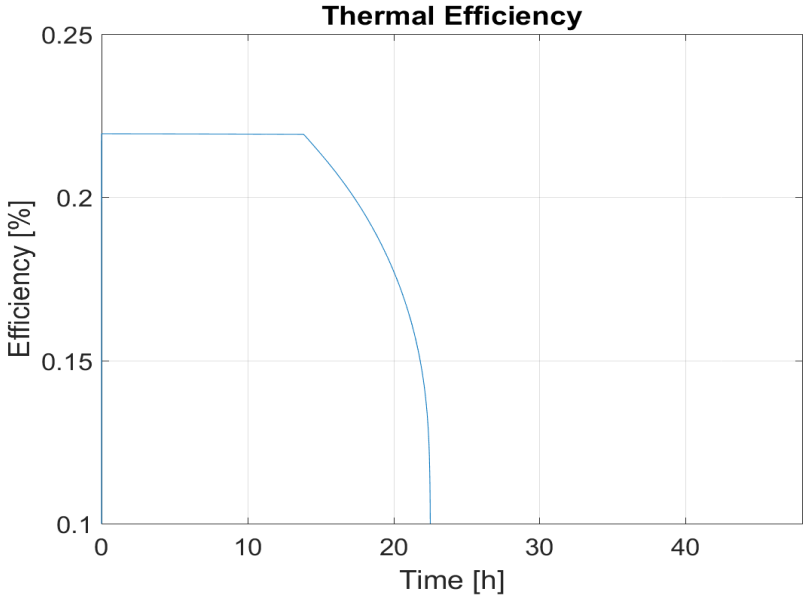

Figure 5.10: Thermal conversion efficiency of the ORC during full power discharge

5.2.3 Parameter study

To assess the impact of variations in the storage parameters on the discharge behavior a parameter study is performed. The parameters that are altered are the length and the amount of heat exchanger pipes. The total amount of storage material is kept constant during all simulations. Both the typical consumption profile and the full power discharge simulations are conducted.

The variables of interest are the same ones discussed in the previous section: discharge time, overall efficiency and the state of charge at the end of discharge. One variable that is added to the analysis: the total meters of pipe needed for the configuration. The most costly component of the storage module is the heat exchanger and is therefore of interest. The results of the consumer profile parameter study are summarized in the following table.

	Consumption profile			
	Time	Efficiency	SOC	pipe m
Starting Setup	42.13	21.3	17.84	10900
Base case	57.5	20.18	3.62	10900
Length +25%	56.87	20.09	3.95	10900
Length -25%	57.5	20.23	3.09	10900
Pipes +10%	57.5	20.23	3.23	12000
Pipes -10%	57	20.04	3.72	9800
Pipes -20%	44.14	21.38	26.57	8720

Table 5.3: Parameter study results for the consumption profile discharge regime

The results for the consumption profile parameter study do not vary greatly from case to case. The large difference between the discharging time of the starting setup and the base case is caused by the shape of the consumption profile. The large peak around the 43 hour mark puts a large strain on the system, causing the starting setup to fail around this point. However, once the simulation passes this point the required power falls again. This allows configurations which reach this point to continue for a considerable amount of time.

The 'Pipes -10%' configuration is able to perform similarly to configurations with larger heat exchanger surfaces. However, further decreasing the amount of heat exchanger surface drastically diminishes the discharge time. This is caused by the phenomenon discussed in the previous paragraph.

	Full power				
	Time	Efficiency	Pumping power [kW]	npipes	pipe m
Starting Setup	18.95	20.75	4.03	545	10900
Base case	22.52	20.75	3.99	545	10900
Length +25%	21.42	20.87	5.86	436	10900
Length -25%	23.53	20.56	2.45	727	10900
Pipes +10%	23.52	20.72	3.59	600	12000
Pipes -10%	21.32	20.77	4.61	490	9800

Table 5.4: Parameter study results for the full power discharge regime

The results of the full power discharge show that increased discharge times are achieved for the 'Length + 25%' and the 'Pipes +10%' scenario's. These scenario's have a lower overall efficiency than the base case. The inverse is true for the 'Length +25%' and the 'Pipes -10%' scenario's. Which have shorter discharge times and longer overall efficiencies.

The explanation for the discharge time differences is found in the pumping power needed for HTF circulation. The scenario's which perform better with regard to the discharge time, both have an increased number of heat exchanger pipes. This results in a lower bulk velocity inside the heat exchanger tubes which greatly influences the needed pumping power. As the overall efficiency drops, the mass flow rate and pressure drop over the storage module increase. The increase in pumping power that follows these changes lowers the overall efficiency until the minimum efficiency of 10% is reached.

5.3 Economic performance

To assess the economic performance added by the electricity storage system, an analysis of the added value of the system is performed. To perform this analysis assumptions need to be made about the value of the different energy streams. For the electricity and heat supplied by the system the average consumption prices of electricity and heat supplied by natural gas, 20 and 6.5 eurocents per kWh respectively [14], are used. The energy used to charge the system is assumed to be costless. This assumption is justified due to the flexible charge capabilities of the system and the expected rise in renewable energy sources.

The added value of a full storage discharge using the consumption profile and under full power is shown in the tables below. The total value is the value of both the thermal and electric energy which was discharged. The added value is the value created by the electric energy. The value and added value for all configurations in both discharge regimes is similar. Only deviating for the configurations where not all energy could be discharged. To place these results into context they

	Consumption profile				
	E_{tot} [MWh]	E_{elec} [MWh]	E_{th} [MWh]	Total Value [$]	Added value [$]
Heat only	42.72	0	42.72	3168	0
Base case	41.17	8.31	32.86	4348	1180
Length +25%	41.03	8.24	32.79	4327	1159
Length -25%	41.40	8.36	33.04	4373	1205
Pipes +10%	41.34	8.36	32.98	4369	1200
Pipes -10%	41.13	8.24	32.89	4334	1166

Table 5.5: Supplied energy and its value during discharge under the consumption profile regime

	Full power				
	E_{tot} [MWh]	E_{elec} [MWh]	E_{th} [MWh]	Total Value [$]	Added value [$]
Heat only	42.72	0	42.72	3168	0
Base case	42.62	8.84	33.77	4545	1378
Length +25%	42.60	8.89	33.71	4528	1384
Length -25%	42.64	8.77	33.87	4528	1368
Pipes +10%	42.63	8.83	33.80	4538	1378
Pipes -10%	30.55	6.35	24.20	3254	93.8

Table 5.6: Supplied energy and its value during discharge under the full power regime

are compared to the system cost of the modeled system as well as its main alternative: Li-ion batteries. The cost of the starting setup was already estimated in chapter 3 and resulted in an estimate of 820.000 USD. For the 20% concrete volume increase these costs only increase slightly

to 830.000 USD. The cost per kWh installed of stationary Li-ion systems differs depending on the energy to power ratio. A typical ratio for such systems is 5:1 which results in an average price of approximately 500 USD/kWh [1].

	Total costs [$]	Value per cycle [$]	Added value [$]	Cycles
Base case	830000	4538.66	1370.4	605.66
Capacity matched	4420000	1931.54	1275.94	3464.12
Power matched	750000	327.75	216.51	3464.12

Table 5.7: Total costs of electricity storage systems along with the value per cycle and the number of cycles needed to offset the costs

The value per cycle refers to the value of the energy sold during the discharge. When the energy sold during the discharge was charged in the normal Ecovat system and supplied as heat this would have created value as well. The added value is the difference between the revenue with and without the electricity storage module. In the final column the number of discharge cycles needed to offset the costs of the electricity storage is listed. It should be noted that the charge and discharge cycles for the Li-Ion systems are considerably shorter than those of the proposed system. The proposed system takes 143 hours to fully charge, or 24 hours to match the storage capacity of the smaller Li-ion system. In contrast the Li-ion systems only takes 5 hours to fully charge.

In the previous analyses it was assumed that the energy to charge the system was procured at no cost. This resulted in a net margin per kWh equal to the selling price per kWh for electricity or heat. In the event that the electricity needs to be bought at higher prices the profit margin shrinks. Because the profit margin for heat energy is smaller than for electricity, system that derive their value from heat energy are more sensitive to rises in the procurement price. This effect is illustrated in figure 5.11 where the number of cycles needed to arrive at the break even point is compared for several conversion efficiencies. Due to its low conversion efficiency the base case is vulnerable to rises in procurement price.

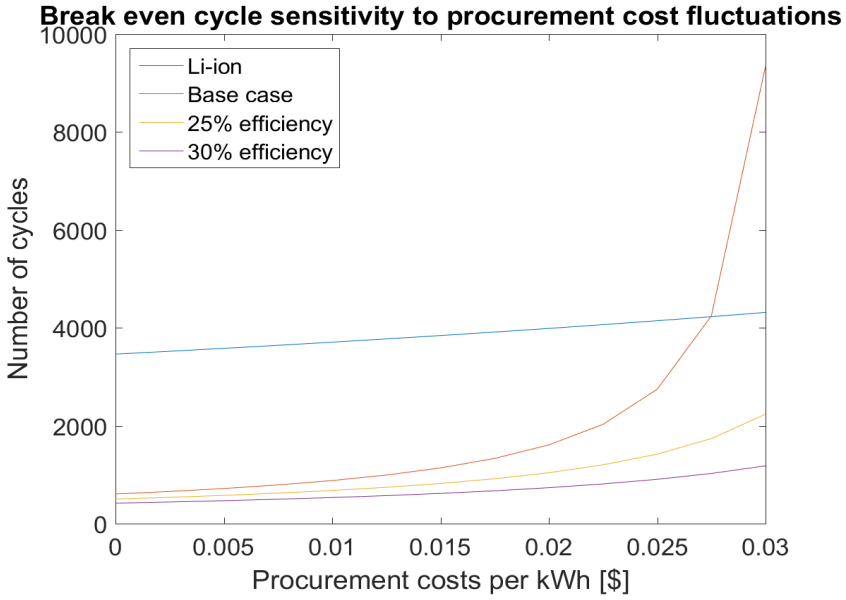

Figure 5.11: Sensitivity of the number of cycles needed to break even to fluctuations in energy procurement costs

Chapter 6

Conclusions

The conclusions of this report are separated into three different sections. The general storage module design, thermodynamic performance of the system and economic performance of the system. After these sections have been addressed recommendations are made for implementation in the Ecovat system and interesting area's for further study.

6.1 General module design

The main performance characteristics of the entire system were profitability and round trip efficiency.

To achieve a profitable system the system needs to be able to perform multiple services for its consumers. The service which aligns best with the current mode of operation of the Ecovat is that of emergency power storage for its connected consumers. The parameters needed for such a system are similar to that of congestion management on the distribution grid. Therefore these two services are selected as the two services to be provided by the system.

The conversion efficiency of the storage module is determined by the used heat engine and the temperature of storage. Of the studied heat engines the Stirling engine has the highest conversion efficiency at moderate temperatures, followed by the ORC and the steam cycle. However, Stirling engines are not widely used in industry, especially for applications exceeding 25 kW. This practical consideration leads to the selection of the ORC as the preferred conversion method. The efficiency reached by ORC's is dependent on the used working fluid and system design. For the simulation a working fluid with a high critical temperature is preferred to allow high inlet temperatures. A recuperator is adopted into the ORC design to increase the temperature of the waste heat stream.

The storage material which results in the lowest costs of the storage module is reinforced concrete. The abundant availability and easy of use of concrete are additional advantages to using concrete. Because concrete is a solid with limited conduction capabilities more heat exchanging surface is needed to supply the desired power.

The final system is designed to supply 300 kW of electric power and has a storage capacity of 35.6 MWh thermal, at a temperature drop of 195 degrees. The total concrete volume is 374 cubic meters in which the heat exchanger consisting of 545, 20 m long, 2.2 cm diameter steel pipes are equidistantly integrated. The investment cost estimate of the storage and conversion module is 830.000 USD. The majority of the costs, 600.000 USD, is attributed to the conversion module. This holds true regardless of the heat engine used for the conversion module.

6.2 Thermodynamic performance

During consumption profile discharge relatively small changes in storage capacity can greatly influence the discharge time. Increasing the amount of storage material by 20% allows the system to operate for 57.5 hours instead of 42 hours, a 36% percent increase. The fluctuating power demands of the consumption profile influence the HTF mass flow rate and inlet temperature considerably. This has a large impact on the conversion efficiency, possibly lowering it below the minimum of 10%.

The dimensional variations indicate that during consumption profile discharge, configurations that limit the flow speed through the heat exchanger perform better. The configurations with shorter and/or more heat exchanger pipes have longer discharge times and higher efficiencies. How much these parameters influence the discharge time does depend greatly on the shape of the discharge profile.

During full power discharge the configurations with limited mass flow rate allow for the longest discharge time. This is mainly caused by the low average pumping power during the discharge cycle.

6.3 Economic performance

Overall the high temperature heat storage module with ORC conversion module provides the most cost effective way to store large quantities of energy. When compared to the most prolific electricity storage technique, Li-ion, the discussed system is the cheaper option by a factor of 5. When compared to the power matched design the installation costs of both the systems are similar.

The number of discharge cycles for the system to break even is 606 as compared to 3465 for the Li-ion systems. So when providing backup power for contracted suppliers the proposed system would reach profitability earlier than comparable Li-ion systems.

Due to the lower conversion efficiency of the proposed HTS system more PTU's are needed to charge the system than comparable Li-ion systems. This increases the likelihood of not being able to charge at reduced costs.

Systems which derive their value from both heat and electricity are more vulnerable to procurement price fluctuations. The per kWh value of heat is lower and therefore increases in procurement price have a large impact on the profit margin and number of cycles needed to break even.

The added value of all electricity storage systems is derived from the difference between the price of electricity and that of heat. Therefore the profitability of the systems is vulnerable to relative price increases of heat compared to electricity.

6.4 Recommendations

6.4.1 Application

Due to the low costs per kWh storage capacity the service of providing backup power can be provided most cost effectively using the HTS setup. Whether the system will prove to be profitable, is however highly dependent on the value which will be attributed to this service. To

further decrease the costs of the installation the power of the conversion module should be minimized. As the most costly aspect of the installation it provides great potential for cost minimization.

For arbitrage and congestion services the large storage capacity of the base case system is not necessary. Therefore the less costly power matched Li-ion system would also suffice. Furthermore, due to the higher conversion efficiency of the Li-ion system, it is able to provide more hours of service within the same period. The system is less vulnerable to fluctuations in procurement price and can achieve a better procurement price due to its shorter charging time. These advantages make the power matched Li-ion system the preferred storage system for arbitrage and congestion services.

6.4.2 Further study

The results of the parameter study indicate that the HTF flow speed strongly influences the needed pumping power, which in turn influences efficiency and discharge time. One parameter which influences the flow rate which was not altered is the inner tube diameter of the heat exchanger tubes. By lowering the overall flow speed the influence of the pumping power on the overall efficiency could be decreased. This allows for more accurate assessment of the influence the other parameter have on the efficiency.

Using the electricity storage as a storage module for residential PV systems could open up an additional revenue stream for the system. Such an application would cause a periodic alternation between partial charge and discharge of the storage module. Its effect on the discharge characteristics could be and interesting next step in the assessment of the viability of the system.
Some of the consumption profile simulations were halted after the conversion efficiency dropped below 10%. The moments the simulations were halted coincided with increasing discharging power. Instead of halting the simulation one can also opt to limit the discharging power. This would mean that not the full power can be supplied to the consumer, but that the discharge can be maintained for longer. When decid

Bibliography

[1] International Renewable Energy Agency. Electricity storage and renewables: Costs and markets to 2030. 55

[2] Ian H. Bell, Jorrit Wronski, Sylvain Quoilin, and Vincent Lemort. Pure and pseudo-pure fluid thermophysical property evaluation and the open-source thermophysical property library coolprop. *Industrial & Engineering Chemistry Research*, 53(6):2498–2508, 2014. 28

[3] Nils Breidenbach, Claudia Martin, Henning Jockenhöfer, and Thomas Bauer. Thermal Energy Storage in Molten Salts: Overview of Novel Concepts and the DLR Test Facility TESIS. *Energy Procedia*, 99(March):120–129, 2016. 15

[4] Topsector Energie. Routekaart Energieopslag. 2015. v, v, v, v, 8, 9, 10, 12

[5] EPRI. Electric Energy Storage Technology Options: A White Paper Primer on Applications, Costs and Benefits. *Epri*, pages 1–170, 2010. v, 4

[6] European Commission. Roadmap 2050. Technical Report April, European Commision, 2012. 1

[7] F. J. Fernández, M. M. Prieto, and I. Suárez. Thermodynamic analysis of high-temperature regenerative organic Rankine cycles using siloxanes as working fluids. *Energy*, 36(8):5239–5249, 2011. v, 25, 26, 31

[8] Antoni Gil, Marc Medrano, Ingrid Martorell, Ana Lázaro, Pablo Dolado, Belén Zalba, and Luisa F. Cabeza. State of the art on high temperature thermal energy storage for power generation. Part 1-Concepts, materials and modellization. *Renewable and Sustainable Energy Reviews*, 14(1):31–55, 2010. v, 14, 22

[9] Florian Heberle and Dieter Brüggemann. Exergy based fluid selection for a geothermal Organic Rankine Cycle for combined heat and power generation. *Applied Thermal Engineering*, 30(11-12):1326–1332, 2010. 25

[10] Elke Klaassen, Elke Klaassen, and Jasper Frunt. Assessing the impact of distributed energy resources on LV grids using practical measurements ASSESSING THE IMPACT OF DISTRIBUTED ENERGY RESOURCES ON LV GRIDS. (October), 2015. 17

[11] Xing Luo, Jihong Wang, Mark Dooner, and Jonathan Clarke. Overview of current development in electrical energy storage technologies and the application potential in power system operation. *Applied Energy*, 137:511–536, 2015. v, 4, 7, 13

[12] Daniel Maraver, Javier Royo, Vincent Lemort, and Sylvain Quoilin. Systematic optimization of subcritical and transcritical organic Rankine cycles (ORCs) constrained by technical parameters in multiple applications. *Applied Energy*, 117:11–29, 2014. 25, 26, 27

[13] Marc Medrano, Antoni Gil, Ingrid Martorell, Xavi Potau, and Luisa F. Cabeza. State of the art on high-temperature thermal energy storage for power generation. Part 2-Case studies. *Renewable and Sustainable Energy Reviews*, 14(1):56–72, 2010. 14

[14] Milieucentraal. Energieprijzen. 54

[15] Riccardo Moro, Piero Pinamonti, and Mauro Reini. ORC technology for waste-wood to energy conversion in the furniture manufacturing industry. *Thermal Science*, 12(4):61–73, 2008. 25

[16] NEDU. Verbruiksprofielen electriciteit. v, 47

[17] Markus Preißinger and Dieter Brüggemann. Thermoeconomic Evaluation of Modular Organic Rankine Cycles for Waste Heat Recovery over a Broad Range of Heat Source Temperatures and Capacities. *Energies*, 10(3):269, 2017. 25

[18] Sylvain Quoilin, Martijn Van Den Broek, Sébastien Declaye, Pierre Dewallef, and Vincent Lemort. Techno-economic survey of organic rankine cycle (ORC) systems. *Renewable and Sustainable Energy Reviews*, 22:168–186, 2013. v, 21

[19] Siemens Brochure. Siemens Organic Rankine Cycle Waste Heat Recovery with ORC. pages 0–25, 2014. 25

[20] E. H. Wang, H. G. Zhang, B. Y. Fan, M. G. Ouyang, Y. Zhao, and Q. H. Mu. Study of working fluid selection of organic Rankine cycle (ORC) for engine waste heat recovery. *Energy*, 36(5):3406–3418, 2011. 25

[21] World Energy Council (WEC). World Energy Resources. page 1028, 2016. v, 5

[22] Chi-jen Yang. *Chapter 2 - Pumped Hydroelectric Storage*. Elsevier Inc., 2016. 6